國 立 交 通 大 學

環 境 工 程 研 究 所

碩士論文

奈米微粒與次微米微粒
在氣膠微粒質量分析儀中的傳輸函數

The Transfer Function of Nanoparticles and Submicron Particles in the Aerosol Particle Mass Analyzer

研 究 生：廖 伯 熙

指導教授：蔡 春 進 博士

中華民國 一〇二 年 六 月

奈米微粒與次微米微粒
在氣膠微粒質量分析儀中的傳輸函數

The Transfer Function of Nanoparticles and Submicron Particles in the Aerosol Particle Mass Analyzer

研 究 生：廖伯熙　　Student：Bo-Xi Liao

指導教授：蔡春進 博士　　Advisor：Dr. Chuen-Jinn Tsai

國 立 交 通 大 學

環境工程研究所

碩 士 論 文

A Thesis

Submitted to Institute of Environmental Engineering

College of Engineering

National Chiao Tung University

in partial Fulfillment of the Requirements

for the Degree of

Master

in

Environmental Engineering

June 2013

Hsinchu, Taiwan, Republic of China

中華民國 一〇二 年 六 月

奈米微粒與次微米微粒
在氣膠微粒質量分析儀中的傳輸函數

研究生: 廖伯熙　　指導教授:蔡春進 博士

國立交通大學環境工程研究所

摘 要

氣膠微粒質量分析儀(APM, Kanomax, Japan)是一部應用離心力與靜電力測量奈米微粒與次微米微粒質量的儀器。過去的文獻指出，微粒在 APM 內部的擴散損失是造成模擬計算值高估實驗數據(例如:質量分佈)的原因，然而至今仍未有研究能將其差異進行量化(Lall et al., 2009, Tajima et al., 2011)。本研究利用二維數值模式研究奈米微粒與次微米微粒在 APM 中的傳輸函數，當假設 APM 中篩選區域的流場為拋物線分佈時，發現本模式的傳輸函數模擬結果與過去採用相同流場的文獻結果相符，但仍舊如過去文獻一樣會高估實驗值。當本研究進一步考慮到因旋轉的篩選區域所引起的強制渦旋及採用更詳細的計算域時，發現旋流出現在 APM 內部的流場，這些出現旋流的區域增強了奈米微粒在 APM 儀器裡的對流擴散損失。本研究的研究結果顯著地提高了模式對 APM 傳輸函數與反應譜的計算準確度。本研究亦根據的數值結果發展出了修正的 Ehara 模式，該模式可更容易及準確地計算傳輸函數。利用本研究所發展出的模式，預期在未來可發展出準確的即時奈米微粒與次微米微粒的質量分佈量測。

關鍵字: 氣膠微粒值量分析儀、APM、傳輸函數、擴散損失、旋流、模式

The Transfer Function of Nanoparticles and Submicron particles in the Aerosol Particle Mass Analyzer

Student: Bo-Xi Liao Adviser: Prof. Chuen-Jinn Tsai

Institute of Environmental Engineering
National Chiao Tung University

Abstract

The Aerosol Particle Mass Analyzer (APM, Kanomax, Japan) is one of the popular instruments to measure the mass of nanoparticles and submicron particles. In previous studies, particle diffusion loss in the APM was speculated to be the reason why simulated response functions for the APM overestimated the experimental data. But no models were available to quantify the differences (Lall et al., 2009, Tajima et al., 2011). This thesis studies the transfer function of the APM by using a 2-D numerical model for nanoparticles and submicron particles. At first, the flow field in the annular classifying region of the APM is assumed to be parabolic. It is found that the transfer functions simulated by the present model are in good agreement with previous studies which also considered the parabolic flow profile. But transfer functions are still overestimated just like previous studies. After solving detailed flow and particle concentration fields in the APM by considering the forced vortex due to the rotating classifying region as well as inlet and outlet regions in the calculation domain, recirculation flow regions are found to exist in the APM. These recirculation flow regions lead to enhanced convection-diffusion loss of nanoparticles in the APM. As a result, the present model improves the accuracy of the transfer functions and response spectra of the APM significantly. Based on the numerical results, a modified Ehara model is developed to ease the calculation of the transfer function. Using these models, it is expected that accurate real time mass distribution measurement of both nanoparticles and

submicron particles can be realized in the future.

Keywords: Aerosol Particle Mass Analyzer, APM, Transfer Function, Diffusion Loss, Recirculation Flow, Model

誌 謝

十萬分地感謝指導教授蔡春進博士的指導與鼓勵，並願意給我機會在適當的壓力下磨練自己，老師的用心指導也讓我在氣膠與環工專業領域方面獲益良多，為我的碩士論文打下好的基礎。口試委員吳宗信教授、黃正雄教授、林文印副教授與預口試委員簡弘民博士的悉心指教與建議，使本論文更加完整。

特別感謝學長冠宇博士無私的經驗分享與專業的支援，使本論文得以完成，學長能駿的耐心討論也使本論文更加完整，學長俊男博士的鼓勵與私房單車路線也使我在巨大壓力下得以放鬆，學長簡志良博士經驗與知識交流也使研究更嚴謹，學長毅弘專業軟體技術傳授也使本論文圖表品質顯著提升，很感謝學長紹銘平時對我的鼓勵與技術上的支援，以及學長栢森無論在畢業前後都予以熱心的幫忙，學長盧緯在我剛入學時給予的寶貴經驗分享，以及學姐香茹、盈禎平日對我的鼓勵也讓我受益良多。也非常地感謝好同窗國瑞的相挺、思帆的支持、瑞喬的幫忙、危涵的鼓勵、Cuc 的英語與經驗分享、葉川的相伴，沒有你們的支持、幫忙與包容，我很幸運有這麼棒的同學;另外也要感謝實驗室的外籍同學羅瑞格、威德、紅幸與 Aditiya 平時的外語訓練與專業知識分享，使我的英文與報告撰寫能力得以顯著提升。助理秉才、偉恩、芳竹與佳芬平時對我的經驗分享與幫助也讓我學到很多。學弟麒鈺、博哲與學妹慧娟的加入也使實驗室的氣氛更加活耀。還有大學同窗家榮在我考碩班時的土地公仙草蜜以及學姐芝萍在我入學後的支援，以及諸多朋友的相挺，使我的碩士研究之路不孤獨。教授高正忠給我的教誨與轉機也讓我受益良多，也很感謝大學恩師教授李志源的栽培與忠告使我能有所發揮。

我也非常非常感謝守護我的健康的唐季祿醫師、江泰平醫師、楊健志醫師、曾興隆醫師，有你們的專業醫療，我才有機會踏進交大完成論文。我也非常感謝女朋友柏安點點滴滴的支持與包容，也給了我無比的溫暖。

最後，將本篇論文獻給我的母親素蓉、父親煌銘與姐姐庭萱，沒有你們的支持，我不會有今天的成就，我很感謝這一切。

Acknowledgement

I very appreciate my adviser, Prof. Chuen-Jinn Tsai, who gave me chance to study with his group and encourages me. The knowledge of aerosol science and technology that professor taught us constructs the foundation of the study. Moreover, with the suggestions given by committees Prof**.** Chong-Sin Gou, Prof. Cheng-Hsiung Huang, Prof. Wen-Yinn Lin, and Dr. Hung-Min Chein, the thesis becomes more complete.

I also appreciate Dr. Guan-Yu Lin's professional supports and valued experience. Without his help, the study cannot be accomplished with such good results. In addition, Neng-Jium, who is always willing to discuss and share the experiences with me, makes the study becomes complete. Chun-Nan's encouragements help me to challenge myself, and Yi-Hung's professional software supports greatly improve the qualities of the figure in the thesis. Chiao-Jin's technology supports are important to the study, and Bo-Sen, Lu-Wei, Shian-Ru, and Ying-Jen also helped me a lot. I also thank my dear classmate Guo-Ruei, Sih-Fan, Jui-Chiao, Wei Han, Cuc, and Ye-Chuan for their supports, encouragements and tolerations. I also appreciate international student Dr. Rodrigo, Virat, Hanh, Aditiya, who are willing to discuss with me about the study and English. Assistant Bing-Tsai, Wei-En, Fang-Ju, and Jia-Fen also helped me a lot. Fresh men Chi-Yu, Po-Che, and Hui-Chuan also enrich the life in laboratory. I also appreciate my college classmate Jia-Rung, and Jhih-Ping, who have helped me when I am a fresh man, and thank my friends who always support me. Prof. Cheng-Chung Kao's suggestions also helped me a lots. Prof. Chi-Yuan Lee's teachings and advisements also play an important role to my life of graduate student.

I specially thank Dr. Jih-Luh Tang, Dr. Tai-Ping Jiang, Dr. Jian-Zhi Yang, and Dr. Xing-Long Ceng for keeping me healthy. I also very appreciate my dear girlfriend Bo-An, who always supporting me and enriching my life.

Finally, I proudly present the thesis to my lovely parents and sister.

Table of Contents

List of Tables

List of Figures

Symbols

A	Cross section area of the classifying region of the APM (m^2)
B	Mobility of particle (m/N · s)
B_c	Mobility of center particle (m/N · s)
$C(d_{p,c})$	Cunningham slip correction factor
d_p	Diameter of particle (nm or m)
$d_{p,c}$	Diameter of center particle (nm or m)
D	The diffusivity or diffusion coefficient (m^2/s)
D_c	Diffusivity or diffusion coefficient of center particles (m^2/s)
D_h	Hydraulic diameter of the classifying region
E	Charge of an electron (C/#)
E_r	Strength of electric field (N/C)
K	Calibrating factor for Gormley and Kennedy equation
L	Length of the classifying region of the APM (m)
M	Mass of the particle (Kg)
n	Number of electron on the particle (#)
$N_{in}(S)$, $N_{out}(S)$	Particle concentration at the APM inlet ($\#/m^3$)
$N_{in}(d_p)$, $N_{out}(d_p)$	Particle concentration at the APM outlet ($\#/m^3$)
$N_{in}(d_p,r)$	Number concentration of particle with diameter d_p at the position r of the inlet of the classifying region ($\#/m^3$)
N_p	Number concentration of particles in the APM ($\#/m^3$).
$N_{out}(d_p,r)$	Number concentration of particle with diameter d_p at the position r of the outlet of the classifying region ($\#/m^3$)
$N_{out}(V)$	Particle concentration at the outlet of the APM operated with voltage V ($\#/m^3$)

$N_p^*(r,z)$	Particle concentration at the position (r,z) (#/m^3)
P	Wet perimeter (m)
$P_{G\&K}$	Particle penetration calculated with Gormley and Kennedy equation
$P'_{G\&K}$	Particle penetration calculated with modified Gormley and Kennedy equation
q	Charge on the particle (C)
Q	Flow rate of the flow entering APM (lpm)
r	Distance from the z axis shown in Fig. 1 to the position of particle (m)
r(S)	Distance from the z axis shown in Fig. 1 to the position of the particle with specific mass S that makes the particle suffer equivalent electrostatic force and centrifugal force (m)
r_1	Inner radius of the classifying region (m).
r_2	Outer radius of the classifying region (m)
r_c	The average of r_2 and r_1, $(r_2+r_1)/2$ (m)
S	Specific mass of particles (Kg/C)
S_c	Specific mass of the center particle (Kg/C)
S_u	Source term derived the Navier-Stoke equation.
$S_1^{\pm}$	Maximum and Minimum specific mass of particles which can pass through the APM (for uniform flow field) (Kg/C)
$S_2^{\pm}$	Maximum and Minimum specific mass of particles that define the shape of the transfer function (for uniform flow field) (Kg/C)
Temp.	Temperature (℃)
$\bar{u}$	Average speed of the flow passing through the classifying region of the APM (m/s).
$\vec{u}$	Velocity of the aerosol flow passing through the APM (m/s).
u_c	Velocity of particle flow induced by centrifugal force (m/s).

u_e	Velocity of particle flow induced by electric force (m/s).
u_r	Velocity of the flow in r direction (m/s)
u_z	Velocity of the flow in r direction (m/s)
$u_z(r)$	Velocity of the flow filed in the classifying region of the APM (m/s)
u_θ	Velocity of the flow in θ direction (m/s)
V	Voltage applied on the APM (volt)
V_c	Voltage of the APM operated with λ_c for chosen specific mass S_c or size $d_{p,c}$ of particles (volt)
X	Parameters of the fitting model
Z_p	Electrical mobility of aerosol (m^2/Volt · s)
$Z_{p,c}$	Electric mobility of center particles (m^2/Volt · s) (Eq. (20))
β_1	Dimensionless number
β_2	Dimensionless number
β_3	Dimensionless number
δ	Half distance of the gap, which is described by $(r_2-r_1)/2$ (m)
ζ	Normalized coordinate in z direction, $\zeta = \frac{z}{L}$
η	Dimensionless number
η_c	Dimensionless number of the center particle
λ_{MFP}	Mean free path of carrier gas (m)
λ	Classification performance parameter (dimensionless number)
λ_c	Classification performance parameter of the center particle (dimensionless number)
μ	Viscosity of the fluid (N · s/m^2)
ρ(S)	Position of particle with specific mass S in normalized r coordinate, $\rho(S) = \frac{[r(S)-r_c]}{\delta}$

ρ_{gas}	Density of carrier gas (Kg/m^3)
σ	The standard deviation of the fitting model (volt)
τ	Relaxation time of particle (s)
τ_c	Relaxation time of the center particle (S)
ω	Rotation speed of the APM (rad/s)
$\Omega_{APM}(d_p)$	APM transfer function of particles with diameter d_p
$\Omega_{APM}(d_p, \omega_{\lambda c}, V)$	Transfer function of particles with diameter d_p passing through the APM operated with rotation speed $\omega_{\lambda c}$ and V
$\Omega_{APM}(S)$	APM transfer function of particles with specific mass S
$\Omega_{APM}(S, \omega_{\lambda c}, V)$	Transfer function of particles with specific mass S passing through the APM operated with rotation speed $\omega_{\lambda c}$ and V
$\Omega'_{APM}(s)$	The APM transfer calculated with the modified Ehara model
$\Omega_{DMA}(d_p, V_{DMA})$	Transfer function of particles with diameter d_p passing through the DMA operated with voltage V_{DMA}

1 Introduction

The Aerosol Particle Mass Analyzer (APM) classifies particles based on their mass to charge ratios or specific masses, denoted as S (Kg/C), by using centrifugal and electrostatic forces (Ehara et al., 1995, Ehara et al., 1996). The direction of the forces is reverse to each other. When the centrifugal force is greater than electrostatic force, the particle will be removed by the centrifugal force. Similarly, when the electrostatic force is greater than the centrifugal force, the particle will be removed by the electrostatic force. Therefore, only narrow range of specific mass of particles can penetrate the APM. Fig. 1 describes the structure of the APM and the concept of the classification (Kanomax Inc.). Because a bipolar charger installed at the APM inlet, nanoparticles are in charge equilibrium condition which allow one to derive the mass of particles from the S for singly charged nanoparticles. The applications of the APM include mass distribution and density measurements, and monodisperse particle generation (Kanomax Inc.).

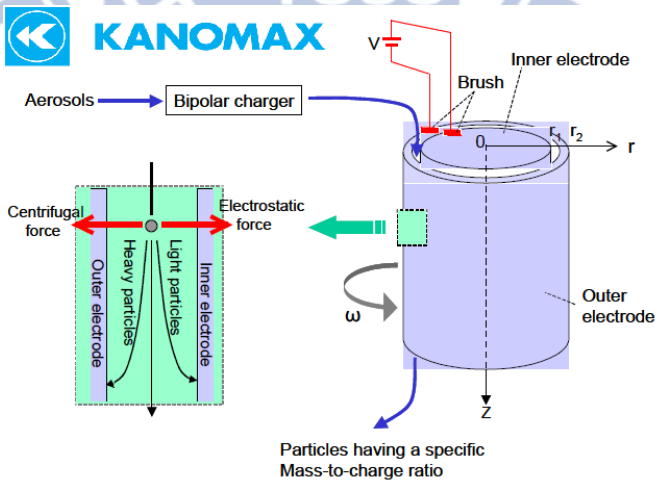

Fig. 1. The schematic diagram of the APM (right) and its mechanism of classification (left) (KANOMAX Inc.).

The following equations describe the condition when the centrifugal force and

electrostatic force are in balance in the APM as well as the specific mass:

$$m \times \omega^2 \times r = \frac{n \times e \times V}{r \times \ln(\frac{r_2}{r_1})} \quad (1)$$

$$S = \frac{m}{n \times e} = \frac{m}{q} = \frac{V}{\omega^2 r^2 \times \ln(\frac{r_2}{r_1})} \quad (2)$$

m: Mass of the particle (Kg)

ω: Rotation speed of the APM (rad/s)

r: Distance from the z axis shown in Fig. 1 to the position of particle (m)

n: Number of electron on the particle (#)

e: Charge of an electron (C/#)

V: Voltage applied on the APM (volt)

r_1: Inner radius of the classifying region (m).

r_2: Outer radius of the classifying region (m)

q: Charge on the particle (C)

The transfer function is the ratio of the particle concentration at the outlet to that at the inlet of the APM. With a specific rotation speed, voltage, and flow rate, each specific mass of particles has a particular transfer function. In addition, if the particle is spherical, the specific mass can be converted to the size of particle with a known density. Eq. (3) describes the transfer function based on the diameter of the particle (denoted as $\Omega_{APM}(d_p)$) or the specific mass of the particle (denoted as $\Omega_{APM}(S)$).

$$\Omega_{APM}(S) = \frac{N_{out}(S)}{N_{in}(S)} \text{ or } \Omega_{APM}(d_p) = \frac{N_{out}(d_p)}{N_{in}(d_p)} \quad (3)$$

In Eq. (3), N_{out} is the particle concentration at the APM outlet, and N_{in} is the particle

concentration at the APM inlet. Fig. 2 is the example of the transfer function. When the rotation speed and the voltage of the APM-3601 are 4487 rpm and 2 volt respectively, only particles with specific mass ranges from 0.2 Kg/C to 0.7 Kg/C can pass through the APM as shown in Fig. 2(a). If the particles are spherical, the specific masses can be converted to the diameters that the particles with diameter ranging between 18 nm to 28 nm can pass through the APM. In Fig. 2, singly charged 22 nm (or 0.37 Kg/C) particles have the maximum transfer function, which is about 0.64. In other words, if there are one hundred 22 nm particles entering the APM with homogeneous concentration at the inlet of the APM, only about sixty of them can pass through the APM. Hence, the transfer function describes the relationship of particle concentrations at the inlet and the outlet of the APM. If particle concentration at the APM inlet is known, one could calculate the outlet particle concentration by using the transfer function.

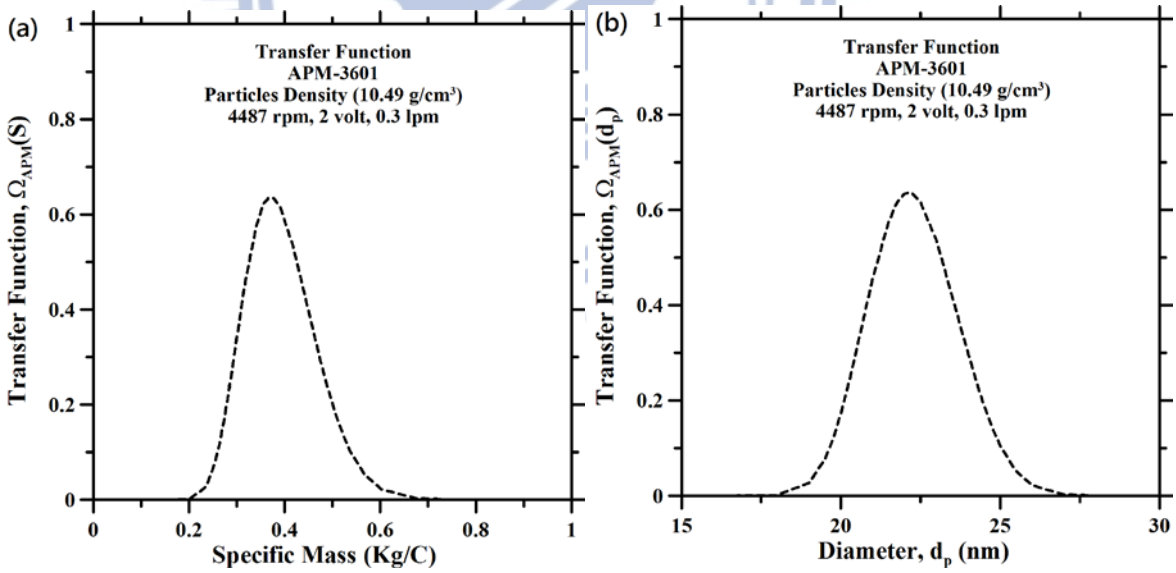

Fig. 2. A typical transfer function of the APM with respective to (a) the specific mass and (b) diameter of spherical particles.

Because the transfer function builds up the relationship between the particles concentrations at the outlet and the inlet of the APM, the calculation of transfer function is

important. Several models have been developed to calculate the transfer function in the literature (Ehara et al., 1995, Hagwood et al., 1995, Ehara et al., 1996, Olfert and Collings 2005). For submicron particles, some models have been verified with experimental data (Ehara et al., 1996, Tajima et al., 2011). For nanoparticles, however, no model has agreed well with the experimental data. Most of the theoretical or numerical models overestimated the peak values of the transfer functions as compared to the experimental data (Lall et al., 2009, Tajima et al., 2011). Previous studies concluded that the differences between the theoretical results and experimental results were due to the diffusion loss caused by Brownian motion (Lall et al., 2009, Tajima et al., 2011). Even when the particle diffusion loss was considered, the models still overestimated the transfer function as compared to experimental data (Olfert et al., 2006, Lall et al., 2009). Hence, the purpose of the study is to improve the accuracy of the transfer function of nanoparticles in the APM.

2 Literature Review

Several models have been developed in the past to calculate the transfer function. Ehara et al., (1995) and Ehara et al., (1996) pioneered the development of the theoretical model for the transfer function based on the trajectories of the particles passing through the APM (Lagrangian approach). Hagwood et al., (1995) presented two numerical models to simulate the transfer function in consideration of effects of the diffusion loss. Based on the convection-diffusion equation, Olfert and Collings (2005) developed the diffusion model of the transfer function. In addition, some studies compared the models with experimental data. Ehara et al., (1996) verified their model with experimental submicron particle data. Lall et al., (2009) applied one of the numerical models developed by Hagwood et al., (1995) to calculate the transfer function, and Tajima et al., (2011) compared APM response spectra simulated by the theoretical model with experimental ones. The methods and the results of

the comparison are described in the following sections.

2.1 Non-Diffusion Model

Theoretical Model

Based on the trajectories of particles passing through the classifying region of the APM, Ehara et al., (1996) developed the original theory (theoretical model) to calculate the transfer function of the APM without considering the Brownian motion of particle. The uniform flow and parabolic flow were applied in the theoretical model respectively. Appendix A contains the details of the assumptions applied in the model.

Ehara et al., (1996) found a dimensionless number λ_c for the APM, which is the dimensionless number of the transfer function for the center particles that achieve force balance of centrifugal force and electrostatic force at the central position (denoted as r_c, which is equal to the average of the r_1 and r_2) between the inner and the outer of the annular cylinders (classifying region). It can be described by Eq. (4) (Ehara et al., 1996). The center particle has the maximum transfer function (roughly). For example, the center particle in Fig. 2 is the particle which has the maximum transfer function. The specific mass and the diameter of the center particle are denoted as $d_{p,c}$ and S_c respectively.

$$\lambda_c = 2\tau_c\omega^2 L/\bar{u} \tag{4}$$

τ_c: Relaxation time of the center particle (S)

L: Length of the classifying region of the APM (m)

$\bar{u}$: Average speed of the flow passing through the classifying region of the APM (m/s).

λ_c describes the peak height (maximum transfer function) and the resolution (relative width) of the transfer function; hence, it is also called classification performance parameter

(Tajima et al, 2011). The lower and narrower transfer function occurs with greater value of λ_c, while the higher and wider transfer function occurs with lower value of λ_c. It should be noted that if the λ_c of the different transfer functions were similar, the height and the shape of those transfer functions were also similar despite differences of rotation speed, voltage or flow rate. Ehara et al., (1996) defined the phenomenon as the similarity rule. Moreover, if the value of λ_c was sufficiently small (ex: less than 0.3), the assumption of the differences between the model in the uniform flow field and the parabolic flow field became insignificant (ex: Maximum height difference can be less than about 4% in transfer function). These features of the small λ_c indicated that the transfer function can be solved with analytical solution; therefore, the small λ_c significantly reduced the complexity of the calculation. Ehara et al., (1996) also verified the model with experimental data of monodisperse 309nm Polystyrene Latex (PSL) (Ehara et al., 1996). In summary, Ehara et al., (1996) described the relationship among the centrifugal force, the electrostatic force and the transfer function through the theoretical model.

2.2 Diffusion Model

Diffusion Loss of Nanoparticles

Nanoparicles have significant Brownian motion compared with submicron particles. The loss of nanoparticles in APM is enhanced due to the Brownian motion. The phenomenon was verified with the numerical models (Hagwood et al., 1995, Olfert and Collings 2005) and the experimental data (Lall et al., 2009 and Tajima et al., 2011). For example, Hagwood et al., (1995) found that the peak of the transfer function of 20nm particles was decreased from about 86% to 20% after considering the diffusion loss of the particles. Tajima et al., (2011) found that results simulated by the model without considering Brownian motion of particles significantly overestimated penetration of 30 nm monodisperse PSL (more than 20% on normalized particle concentration). In addition, the degree of overestimation

became insignificant for submicron particles (Fig. 3). The different levels of overestimation showed the effects of the Brownian motion. In sum, the Brownian motion of nanoparticles indeed has great impact on the transfer function.

Numerical Model

The theoretical model developed by Ehara et al., (1996) was accurate for submicron particles, but it overestimated the transfer function for nanoparticles due to the assumption neglecting the Brownian motion. Some numerical methods were developed to calculate the transfer function with considering the Brownian motion of particles (Hagwood et al., 1995, Olfert and Collings 2005).

Hagwood et al., (1995) developed two numerical methods, the Stochastic Differential Equation (SDE) and the Monte Carlo method (MC), to simulate the transfer function in consideration of the Brownian motion. The former calculated the transfer function based on the probability of particles passing through the APM, while the latter applied the Gaussian random variables to describe the Brownian motion. Appendix A contains some important assumptions applied to the models. The results calculated by these models showed the significant effects of the Brownian motion of nanoparticles on the transfer function.

Another numerical model was developed by Olfert and Collings (2005), which was based on the convection-diffusion equation. The study also found another dimensionless number η as described in Eq. (4). The η took the diffusivity of particles in to consideration. The effects of diffusion become important when $|\eta_c|$ of the APM applied in the study was approximately less than 10 (Olfert and Collings 2005, Olfert et al., 2006).

$$\eta_c = \frac{2\delta^2 \tau_c \omega^2}{D_c} \tag{5}$$

δ: Half distance of the gap, which is described by $(r_2-r_1)/2$ (m)

D_c: Diffusivity or diffusion coefficient of center particles (m^2/s)

2.3 Verification of the Models

Up to now, several models were developed. Some of the models have been compared with experimental data (Ehara et al., 1996, Olfert et al., 2006, Lall et al., 2009, Tajima et al., 2011); however, no model has accurately agreed with experimental data for nanoparticles even if the effects of Brownian motion were considered in the model.

$$N_{out}(V) = \int N_{in}(S)\Omega_{APM}(S,V)dS \quad (6)$$

Ehara et al., (1996) calculated the number concentration of monodisperse particles passing through the APM (Eq. (6)). In Eq. (6), the particle concentration at the APM outlet, denoted as $N_{out}(V)$, is the function of voltage. The particle concentration at the APM inlet was considered the function of the specific mass (denoted as $N_{in}(S)$) which was assumed to be proportional to the δ function, and the transfer function of the APM was denoted as the function of the specific mass and voltage (denoted as $\Omega_{APM}(S,V)$). The rotation speed of the APM was fixed, while the voltage of the APM was shifted to scan the specific mass distribution of the particles. The theoretical relative particle concentration, which is the ratio of the total particle concentration at the APM outlet to that at the APM inlet, was calculated with different voltage and compared with the experimental one. Good agreement of the comparisons between the experimental data (monodisperse 309 nm PSL) and the simulated results showed the validity of the theoretical model.

Since the theoretical model developed by Ehara et al., (1996) neglected the Brownian motion of particles, the model is not suitable to nanoparticles. Tajima et al., (2011) applied

the model disregarding the Brownian motion of particles to simulate the APM response spectra which is same as the relative particle concentration calculated in Ehara et al., (1996). The flow field of the model was assumed to be parabolic. Different to Ehara et al., (1996), Tajima et al., (2011) considered the size distribution of monodisperse PSL at the APM inlet more carefully as described in Eq. (7). The size distribution of the particles at the inlet of Differential Mobility Analyzer (DMA) were considered the Gaussian distribution (denoted as $N_0(d_p)$) based on the mean and standard deviation of size of size standard PSL. Moreover, the particles classified by the DMA ($N_{in}(d_p)$) is considered the product of the $N_0(d_p)$ and the transfer function of the DMA (denoted as Ω_{DMA}). V_{DMA} is the voltage applied to the DMA. The rotation speed of the APM was fixed based on the specific λ_c, while the voltage was shifted to scan the specific mass distribution of monodisperse PSL, and the normalized particle concentration were calculated and compared with the experimental one.

$$N_{in}(d_p) = N_0(d_p) \times \Omega_{DMA}(d_p, V_{DMA}) \tag{7}$$

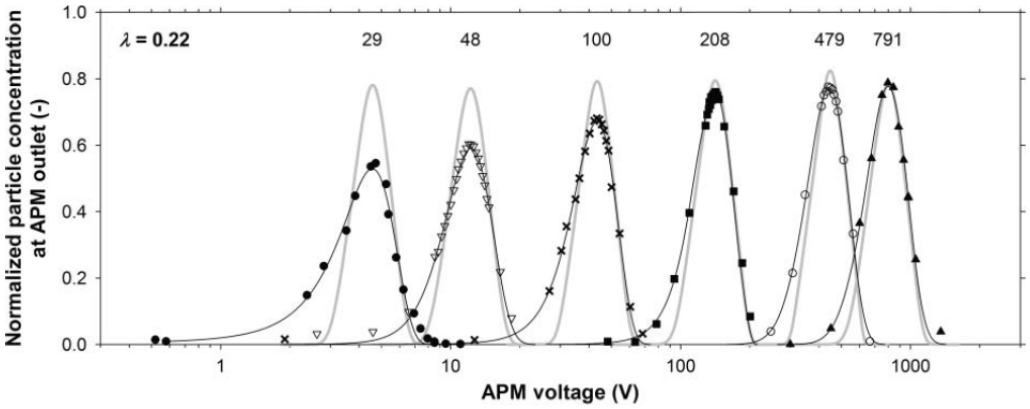

Fig. 3. Theoretical and experimental normalized particle concentration. (Tajima et al., 2011)

Fig. 3 showed the results of comparisons presented in Tajima et al., (2011). The number on each curve was the size of the monodisperse PSL. The thick grey lines were the simulated results, and the thin black lines fitted the experimental data (points) with the least

square fitting method. Differences between the simulated results and experimental data became significant for PSL less than 100 nm. Tajima et al., (2011) concluded that the differences (overestimations) were caused by diffusion loss.

Lall et al., (2009) applied the MC method (Hagwood et al., 1995) to calculate the APM transfer function with the assumption of the parabolic flow field, and they also calculated the particle concentration at APM outlet with the manner similar to the manner did in Tajima et al., (2011) as described in Eq. (6) and (7). Different from Tajima et al., (2011), Lall et al., (2009) considered the N_0 as the constant function and applied the triangular function to the transfer function of the DMA. Comparing to experimental data, Lall et al., (2009) found the simulated results overestimated the penetration for nanoparticles (60 nm, 100 nm PSL) and submicron particles (300 nm PSL). Lall et al., (2009) concluded that was due to diffusion losses and transport losses.

Olfert et al., (2006) verified the model presented in Olfert and Collings (2005). Instead of the APM, the major objective of the study for Olfert and Collings (2005) is the Couette Centrifugal Particles Mass Analyzer (CPMA). Because the only difference between two instruments is the rotation speeds of the inner and outer cylinders, while the cylinders of the APM have the same rotation speed, the CPMA is very similar to the APM. The different rotation speed of cylinders of the CPMA was applied in order to achieve the stabler state of the classification (decrease the loss of particles during the classification). Since the APM is very similar to the CPMA, the diffusion model developed by Olfert and Collings (2005) not only available to the CPMA but also available to the APM. Olfert et al., (2006) compared the model of the CPMA with experimental data. The assumption of parabolic flow field was made in the model, and of assuming that particles at the APM inlet are strict monodisperse (particles are in same size). For 50 nm PSL, the diffusion model significantly overestimated the transfer function compared to the experimental data. Olfert et al., (2006) concluded that the overestimation was due to the particle diffusion. Because the model of the CPMA is

very similar to the model of the APM, we consider that the result concluded for the CPMA in Olfert et al., (2006) would also be available to the APM.

In sum, for submicron particles, some models have been verified by the experimental data (Ehara et al., 1996, Tajima et al., 2011). For nanoparticles, however, no model has agreed well with experimental data. Table 1 summarizes the performance of previous transfer function models.

Table 1 The summary of the performance of previous models

Performance of Previous Model				
Theoretical Model			Experimental Verification	
Previous Studies	Solution Form	Diffusion Loss Consideration	Submicron Particles (100nm<d_p<1000nm)	Nanoparticles (d_p<100nm)
Ehara Model (Ehara et al., 1996)	Analytical or Numerical	No	Accurate[1]	Overestimated[1]
S.D.E Model (Hagwood et al., 1995)	Numerical	Yes	No Study	No Study
M.C. Model (Hagwood et al., 1995)	Numerical	Yes	Overestimated[1]	Overestimated[1]
Diffusion Model (Olfert and Collings 2005)	Numerical	Yes	Overestimated[2]	Overestimated[2]

1: Aerosol Particle Mass Analyzer (APM, Inner and Outer Cylinders rotates with same speed)
2: Couette Centrifugal Particle Mass Analyzer (CPMA, Inner and Outer Cylinders rotates with different speed)

3 Numerical Method

A 2-D numerical model developed by our laboratory is applied to simulate the transfer function of the APM. The preliminary verification of the model is conducted with comparing the simulated transfer function with ones done by previous models with simple calculation domain (the classifying region of the APM) and assumption of parabolic flow field. After the preliminary verification, the model is further improved by extending calculation domain from classifying region to whole region in the APM and by considering detailed flow field based on the Navier-Stokes equations. The improved model is used to compare with the experimental data shown in Tajima et al., (2011) as the advanced verification.

3.1 2-D Numerical Model

Governing Equation

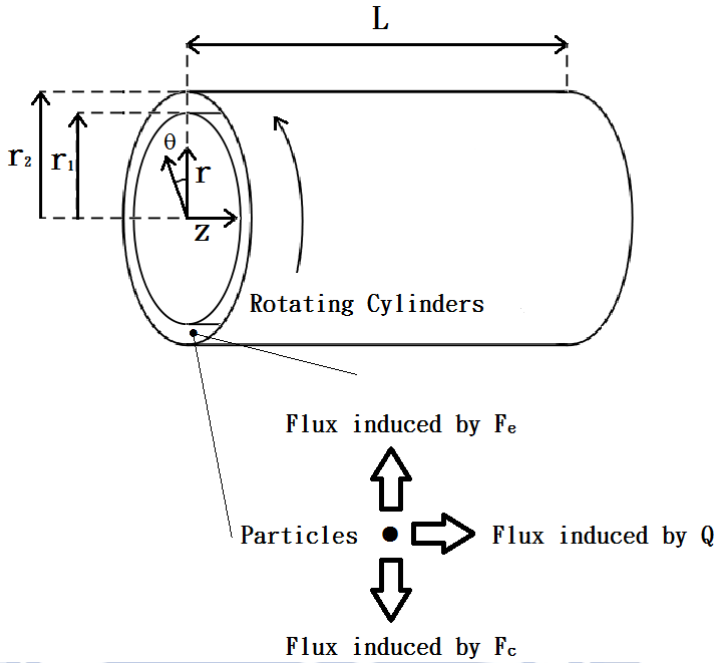

Fig. 4. Scheme of the APM and the flux of particles induced in the APM.

Fig. 4 shows the principle of the model applied in the model. Charged particles were introduced in the classifying region of the APM (the space between the closely-spaced annular cylinders). Particles passing through the region are classified by the centrifugal force F_c and electrostatic force F_e. In Fig. 4, L is the length of the APM. Three directions of flux in the classifying region are considered. First one is the flux induced by the carrier gas. Particles move with the direction of flow in the APM. Second one is for the particles of which F_e is greater than F_c, the flux toward the inner cylinders is induced. Third one is for particles of which F_e is smaller than F_c, the flux flowing toward the outer cylinders is induced. The flux describe the particles which are classified by the APM.

The governing equation applied in the model is based on the convection-diffusion equation. The general equation of the convection-diffusion equation is

$$\frac{\partial N_p}{\partial t} = \nabla \cdot \left(D \nabla N_p\right) - \nabla \cdot \left(\vec{u} N_p\right). \quad (8)$$

N_p: Number concentration of particles in the APM (#/m^3).

$\vec{u}$: Velocity of the aerosol flow passing through the APM (m/s).

It is considered that there is no source, sink or chemical reaction in the APM classifying region. The study considers that the flow in the APM is isothermal and steady. Since the Mach number of the flow is much less than 0.5 (ex: 0.0046 for the APM-3601 or 0.015 for the APM-3600), the carrier gas (ex: air) is considered as incompressible fluid. In addition, the classification of the APM is assumed to be steady ($\frac{\partial N_p}{\partial t}$=0). Because centrifugal force and electrostatic force do not change in θ direction, the particle motion in θ direction and the flow field in θ direction are neglected in the model (u_θ=0). Finally, the governing equation of 2-D model for the transfer function is

$$\frac{\partial [u_r + (u_c - u_e) N_p]}{\partial r} + \frac{\partial (u_z N_p)}{\partial z} = D \left[\frac{1}{r}\frac{\partial}{\partial r}\left(r \frac{\partial N_p}{\partial r}\right) + \frac{\partial^2 N_p}{\partial z^2}\right]. \quad (9)$$

u_r: Velocity of flow in r direction (m/s)

u_z: Velocity of flow in z direction (m/s)

u_c: Velocity of particle flow induced by centrifugal force (m/s).

u_e: Velocity of particle flow induced by electric force (m/s).

r: Distance between the aerosol and the axis of the APM (m).

Eq. 9 is further rewritten with the detailed description of u_e and u_c, as described in Eq. (10) and (11), to be Eq. (12).

$$u_c = \tau r\omega^2 = mBr\omega^2 \tag{10}$$

$$u_e = Z_p E_r(r) = Z_p \frac{V}{r \ln\frac{r_2}{r_1}} \tag{11}$$

$$\frac{\partial[(\tau r\omega^2 - Z_p E_r)N_p]}{\partial r} + \frac{\partial(u_r N_p)}{\partial r} + \frac{\partial(u_z N_p)}{\partial z} = D\left[\frac{1}{r}\frac{\partial}{\partial r}\left(r\frac{\partial N_p}{\partial r}\right) + \frac{\partial^2 N_p}{\partial z^2}\right] \tag{12}$$

τ: Relaxation time of particle (s)

B: Mobility of particle (m/N · s)

E_r: Strength of electric field (N/C)

Z_p: Electrical mobility of aerosol (m^2/Volt · s)

Several dimensionless parameters are applied to obtain the dimensionless form of Eq. (12). These parameters are listed in Eq. (13) to Eq. (20) respectively.

$$N_p^* = \frac{N_p}{N_{in}} \tag{13}$$

$$u_z^* = \frac{u_z}{\bar{u}} \tag{14}$$

$$u_r^* = \frac{u_r}{\bar{u}} \tag{15}$$

$$r^* = \frac{r}{4\delta} \tag{16}$$

$$z^* = \frac{z}{4\delta} \tag{17}$$

$$Z_p^* = \frac{Z_p}{Z_{p,c}} \tag{18}$$

$$\tau^* = \frac{\tau}{\tau_c} \tag{19}$$

$$D^* = \frac{D}{D_c} \tag{20}$$

N_{in}: Particle concentration at the APM inlet (#/m^3)

$Z_{p,c}$: Electric mobility of center particles (m^2/Volt · s) (Eq. (21))

B_c: Mobility of center particle (m/N · s)

$d_{p,c}$: Diameter of center particle (m) (Eq. (22))

$C(d_{p,c})$: Cunningham slip correction factor (Eq. (23))

$$Z_{p,c} = qB_c = ne\frac{C(d_{p,c})}{3\pi\mu d_{p,c}\kappa} \tag{21}$$

$$d_{p,c} = \left(\frac{6Vne}{\pi\rho_{gas}r_c^2\omega^2\ln\left(\frac{r_2}{r_1}\right)}\right)^{\frac{1}{3}} \tag{22}$$

$$C(d_p) = 1 + \left(\frac{2\lambda_{MFP}}{d_p}\right)\left[1.142 + 0.558\exp\left(\frac{-0.999d_p}{2\lambda_{MFP}}\right)\right] \tag{23}$$

ρ_{gas}: Density of carrier gas (Kg/m^3)

λ_{MFP}: Mean free path of carrier gas (m).

The 4δ shown in the denominator of Eq. (16) and (17) is the characteristic length of the APM. In the study, the hydraulic diameter of the classifying region (D_h) is considered the characteristic length (Eq. 24). In Eq. (24), A is the cross section area of the classifying region of the APM (m^2), and P is the wet perimeter, the sum of the circumferences of inner and outer radius of the classifying space (m).

$$D_h = \frac{4A}{P} = \frac{4\pi(r_2^2 - r_1^2)}{2\pi(r_2 + r_1)} = 2(r_2 - r_1) = 4\delta \tag{24}$$

With Eq. (13)~(20), the dimensionless form of governing equation is obtained as

$$\frac{\partial[(\tau_c\tau^*\omega^2 r^* 4\delta)(N_0 N_p^*)]}{4\delta\,\partial r^*} - \frac{\partial\left[\left(Z_p^* Z_{p,c}\frac{K}{4\delta r^*}\right)(N_0 N_p^*)\right]}{4\delta\,\partial r^*} + \frac{\partial[(\bar{u}u_r^*)(N_0 N_p^*)]}{4\delta\,\partial r^*} + \frac{\partial[(\bar{u}u_z^*)(N_0 N_p^*)]}{4\delta\,\partial z^*}$$
$$= D_c D^* \left[\left(\frac{1}{4\delta r^*}\right)\frac{\partial}{4\delta\,\partial r^*}\left(4\delta r^* \frac{N_0\,\partial N_p^*}{4\delta\,\partial r^*}\right) + \frac{N_0}{(4\delta)^2}\frac{\partial^2 N_p^*}{\partial z^{*2}}\right]. \quad (25)$$

Eq. (25) can be further rewritten to be Eq. (26).

$$\tau_c\omega^2 \frac{\partial[\tau^*(r^*)(N_p^*)]}{\partial r^*} - \frac{Z_{p,c}K}{(4\delta)^2}\frac{\partial\left(Z_p^*\frac{N_p^*}{r^*}\right)}{\partial r^*} + \frac{\bar{u}}{4\delta}\frac{\partial[u_r^* N_p^*]}{\partial r^*} + \frac{\bar{u}}{4\delta}\frac{\partial[u_z^* N_p^*]}{\partial z^*}$$
$$= \frac{D_c}{(4\delta)^2}\left[D^*\left(\frac{1}{r^*}\right)\frac{\partial}{\partial r^*}\left(r^*\frac{\partial N_p^*}{\partial r^*}\right) + D^*\frac{\partial^2 N_p^*}{\partial z^{*2}}\right] \quad (26)$$

where K is $\frac{V}{\ln\left(\frac{r_2}{r_1}\right)}$. After dividing Eq. (26) by $\frac{\bar{u}}{4\delta}$, we can obtain

$$\frac{4\delta\tau_c\omega^2}{\bar{u}}\frac{\partial[\tau^*(r^*)(N_p^*)]}{\partial r^*} - \frac{Z_{p,c}K}{4\delta\bar{u}}\frac{\partial\left(Z_p^*\frac{N_p^*}{r^*}\right)}{\partial r^*} + \frac{\partial[u_r^* N_p^*]}{\partial r^*} + \frac{\partial[u_z^* N_p^*]}{\partial z^*}$$
$$= \frac{D_c}{4\delta\bar{u}}\left[D^*\left(\frac{1}{r^*}\right)\frac{\partial}{\partial r^*}\left(r^*\frac{\partial N_p^*}{\partial r^*}\right) + D^*\frac{\partial^2 N_p^*}{\partial z^{*2}}\right]. \quad (27)$$

Three dimensionless numbers are found from Eq. (27) as described in Eq. (28)~(30).

$$\beta_1 = \frac{4\delta\tau_c\omega^2}{\bar{u}} \quad (28)$$

$$\beta_2 = \frac{Z_{p,c}V}{4\delta\bar{u}\ln\left(\frac{r_2}{r_1}\right)} \quad (29)$$

$$\beta_3 = \frac{D_c}{4\delta\bar{u}} = \frac{1}{Pe} \quad (30)$$

The β_1 includes the rotation speed of the APM, the average velocity of the carrier gas, and the relaxation time of the center particle, which is almost same as the dimensionless number λ found by Ehara et al., (1996) (Eq. (4)). The β_2 considers the electric mobility of the center

particle, the strength of the electric field, and the average velocity of the carrier gas. β_1 and β_2 are dependent to each other through the force balance of F_c and F_e of the center particle. The β_3 includes the diffusivity of the center particle. It is considered the reciprocal Peclet number (denoted as Pe). Greater value of β_3 represents the stronger effects of the Brownian motion. Furthermore, it is found that the ratio of β_1 to β_3 is just equal to eight times of the dimensionless number η (Eq. (4)), which is described in Eq. 31. Since the β_1 and β_1/β_3 are similar to the λ_c and η respectively, the properties of λ_c and η should be also applicable to the β_1 and β_1/β_3. For example, the similarity rule found by Ehara et al., (1996) described that when the λ_c of the transfer function were similar, the height and shape of the transfer functions were similar too. The rule should be available on the β_1 too. Another example is that Olfert et al., (2006) mentioned that the effects of the diffusion are important when the absolute value of η_c is less than 10 or the absolute value of β_1/β_3 is less than 80 for the simulated APM. In sum, three dimensionless numbers are derived from governing equation, and the dimensionless numbers can cover ones presented in previous studies.

$$\frac{\beta_1}{\beta_3} = \frac{(4\delta)^2 \tau_c \omega^2}{D_c} = 8 \times \left(\frac{2\delta^2 \tau_c \omega^2}{D_c}\right) = 8\,\eta_c \tag{31}$$

In sum, the governing equation has been developed based on the convection-diffusion equation. The governing equation will be applied to study the transfer function of nanoparticle and submicron particle of the APM. Moreover, three dimensionless numbers (β_1, β_2 and β_3) are found. The β_1 is related to the rotation speed, the β_2 is related to the voltage, and the β_3 is related to the diffusivity of the particles. The obtained dimensionless numbers can be similar to the ones presented in previous studies (ex: λ_c, η_c); hence, the characteristics of the λ_c and η_c should be also available to our dimensionless numbers β_1 and β_1/β_3.

Dimensionless Numbers for two Different APM models

To compare the performance between different APMs (Model 3600, Model 3601, Kanomax Japan Inc.), dimensionless numbers β_1, β_2 and β_3 are applied to characterized their performances. The geometry and the performance of the APMs are listed in table 2. The shape of particle is considered spherical; hence, the mass of particle can be easily converted to size with known particle density (ex: 1.05 g/cm^3).

Table 2 The geometry and performance of the APMs (Kanomax Inc.)

APM Model (Kanomax Inc.)	**r_1 (m)**	**r_2 (m)**	**Length of APM (m)**	**Voltage (volt)**	**Rotation Speed (rpm)**	**Carrier gas Flow Rate (lpm)**
APM-3600	0.05	0.052	0.25	0.3~2000	50~9500	0.3
APM-3601	0.024	0.025	0.1	0.3~2000	1000 ~14000	0.3

Fig. 5 shows the results of the characterization. The black lines are the values of the dimensionless numbers of the APM-3600, while the red lines are the values of the dimensionless numbers of the APM-3601. In Fig. 5(a) and 5(b), the dashed lines indicate the maximum values of the dimensionless numbers for each size of particles, and the solid lines indicate the minimum values of the dimensionless numbers.

In Fig. 5(a), the range of the β_1 of the APM-3600 is wider than that of the APM-3601. The available maximum rotation speed of the APM-3601 (14000 rpm) is higher than that of the APM-3600 (9500 rpm), yet the APM3600 can perform with wider range of the β_1 than the APM-3600 due to different size and geometry of the classifying regions. For example, when the rotation speed are the same, the radius of classifying region of the APM-3600 is longer than that of the APM-3601, it makes the APM-3600 has stronger centrifugal force compared

to the APM-3601. Moreover, when the APMs operated with same flow rate (0.3 lpm), the slower average velocity $\bar{u}$ of carrier gas makes the APM-3600 has larger β_1 compared to the APM-3600.

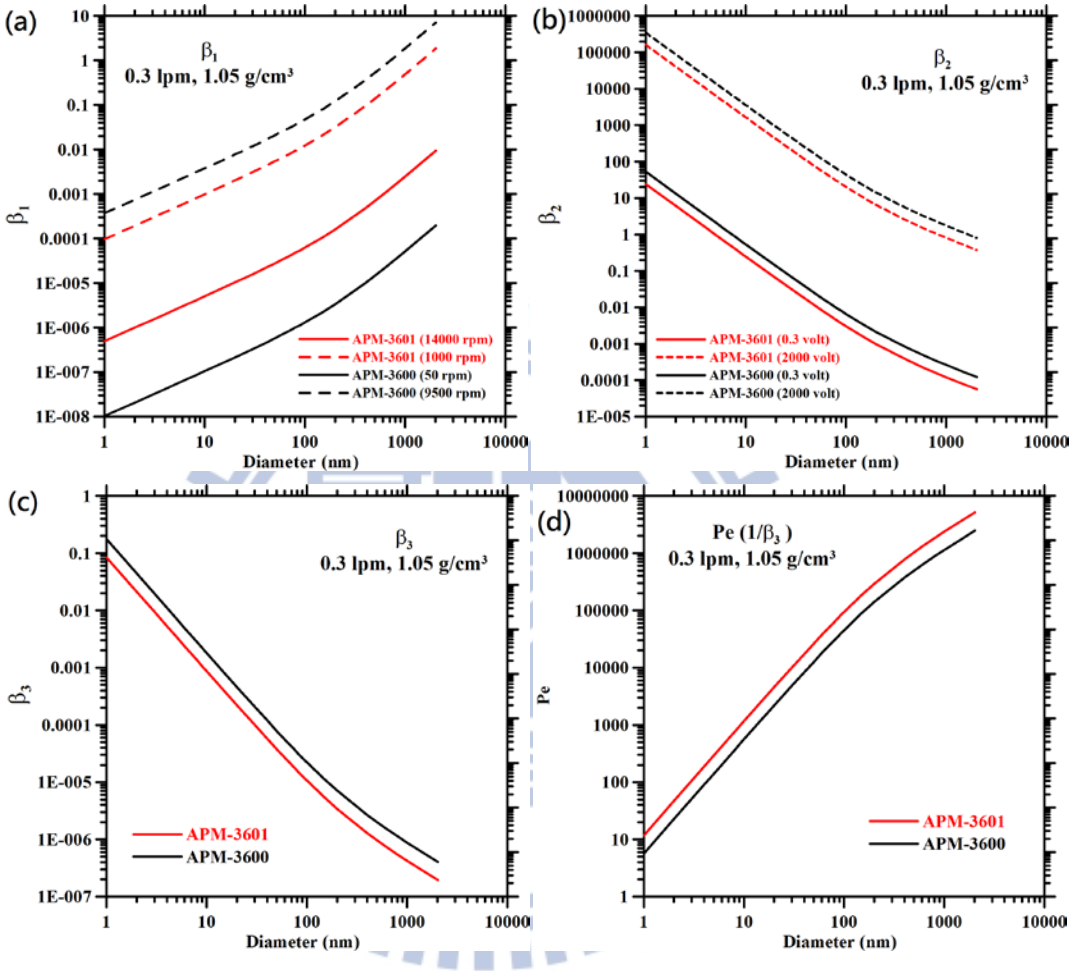

Fig. 5. The ranges of the dimensionless numbers for APM-3600 and APM-3601

In Fig. 5(b), although the available range of voltage of both APMs is the same, the β_2 of the APM-3600 can be higher than that of the APM-3601. We conclude that it is due to slower $\bar{u}$ of the APM-3600 compared to that of the APM-3601 when the flow rates of both APMs are the same. Hence, it is concluded that the APM-3600 can perform with the higher β_2 compared with the APM-3601. Fig. 5(c) and 5(d) show the relationship between the size of the particles and the β_3 and Pe respectively. The β_3 of the APM-3601 are lower than of the

APM-3600. It is because that the gap between the outer and inner radius of classification space of the APM-3601 is narrower than that of the APM-3600. The narrower gap makes the flow velocity of the APM-3601 higher than of the APM-3600; hence, the retention time (diffusion time) of particles passing through the APM-3601 is decreased.

In sum, the APM-3600 can operate with wilder range of the β_1 and higher β_2 compared to the APM-3601, while the APM-3601 is more suitable to operate with smaller nanoparticles (less diffusion loss) compared to the APM-3600.

3.2 Model with Classifying Region Domain and Parabolic Flow Profile

In this section, the governing equation presented in chapter 3.1 is applied to build up the model. The calculation domain of the model is the classifying region of the APM and parabolic flow field is applied. The transfer functions simulated by the model are compared with ones simulated with previous models. The comparison is considered as the preliminary verification of our model. Based on the good agreements of the comparison, the model presented in the section is considered the representative of the previous models.

Calculation Domain

In Fig. 6, the dark orange area is the classifying region, which is the space between the inner and outer closely-spaced annular cylinders. Several studies considered the classifying region the calculation domain of their models (Hagwood et al., 1995, Ehara et al., 1996, Olfert and Collings 2005). To verify our model, the calculation domain of our model is defined to be the classifying region as previous studies did.

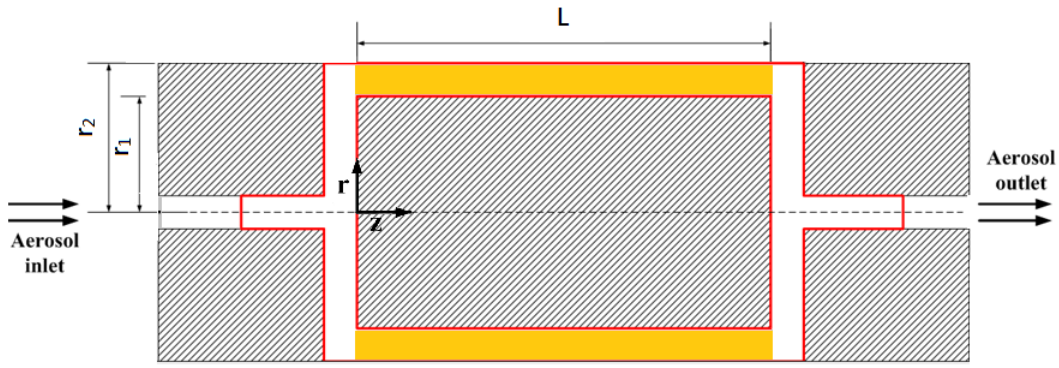

Fig. 6. Caculation domain is the annular classifying region of the APM (dark orange area). The area enclosed by thick red lines is the rotating region.

Flow Field

Because previous studies usually made the assumption of laminar parabolic flow field for their models (Hagwood et al., 1995, Ehara et al., 1996, Olfert and Collings 2005), we apply the same assumption of the flow field for the model. Eq. (32) is applied to describe the parabolic flow field in the classifying region of the APM.

$$u = u_z(r) = \frac{3}{2}\bar{u}\left[1 - \left(\frac{r - r_c}{r_2 - r_1}\right)^2\right] \quad (32)$$

r_c: The average of r_2 and r_1 (m), $(r_2+r_1)/2$

Eq. (33) describes the transfer function, Ω_{APM}, for particles with diameter d_p. In eq. (33), the number concentration of the particles at the APM inlet $N_{in}(d_p, r)$ is considered homogeneous, while the number concentration of the particles at the APM outlet $N_{out}(d_p, r)$ is solved numerically by the SIMPLER algorithm (Semi-Implicit Method for Pressure-Linked Equations) (Patankar 1980, Lin et al., 2010).

$$\Omega_{APM}(d_p) = \frac{2\pi \int_{r_1}^{r_2} N_{out}(d_p,r)u_z(r)dr}{2\pi \int_{r_1}^{r_2} N_{in}(d_p,r)u_z(r)dr} \quad (33)$$

Boundary Condition

Eq. (34) and (35) describe the boundary conditions of the model. $N_p^*(r,z)$ is the normalized particle concentration, the ratio of particle concentration at the outlet to the inlet of the APM classifying region, at the position (r,z). $N_p^*(r,0)$, the normalized particle concentration at the inlet of classifying region, is considered as 1. In addition, because particle contacting the walls in the classifying region is removed, particle concentration at the walls is considered zero (removed by the APM).

$$N_p^*(r,0) = 1 \quad \text{for } r_1<r<r_2 \quad (34)$$

$$N_p^*(r_2,z) = N_p^*(r_1,z) = 0 \quad (35)$$

Compared with Previous Studies

The transfer functions simulated with the model presented in this section are compared with ones simulated with three previous models respectively, which are the theoretical model developed by Ehara et al., (1996), the numerical models presented in Hagwood et al., (1995) and the diffusion model developed by Olfert and Collings (2005). To simplify the calculation, the particle is assumed spherical. The result of the comparisons is considered as the preliminary verification of the model.

For the comparisons of our model and the theoretical model (Ehara et al., 1996) and the numerical models (Hagwood et al., 1995), the parameters of the models are set to be same as the ones set in Hagwood et al., (1995) (table 3). For the comparison of our model and the diffusion model developed by Olfert and Collings (2005), the parameters of the models are set to be same as the ones used in Olfert and Collings (2005) (table 3). Because pressure and

temperature applied in some previous studies were unknown, we assumed the atmospheric pressure and 25 ℃ for these parameters.

Table 3 Parameters presented in compared papers.

References	r_1 (m)	r_2 (m)	L (m)	Pressure (atm)	Temp. (◦ C)	Q (lpm)	$\rho_{aerosol}$ (Kg/m^3)
Hagwood et al., (1995)	0.1	0.101	0.2	(assumed 1)	(assumed 25)	0.5	1000
Olfert and Collings (2005)	0.1	0.103	0.2	(assumed 1)	22	0.5	1000

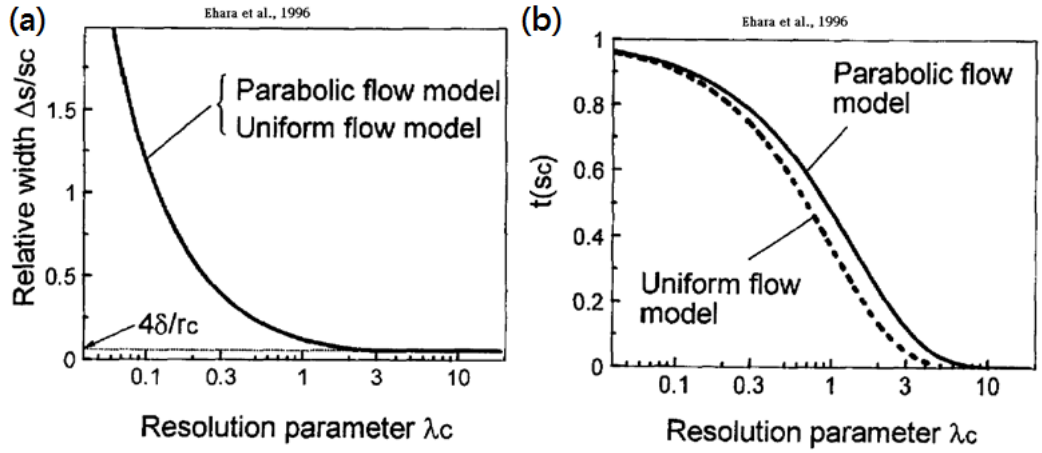

Fig. 7. (a) The relative width and (b) the maximum height of the transfer functions for different flow field applied to the Ehara model (Ehara et al., 1996).

It should be noted that Ehara et al., (1996) found that if the value of the λ_c is small (less than about 0.5), there is no significant difference between the transfer functions simulated by the Ehara model with uniform flow field and parabolic flow field (Fig. 7). The λ_c of the transfer function applied in the comparison of our model and Ehara model is about 0.044, which is much lower than the 0.5. Moreover, applying the uniform flow field makes the transfer function available to be solved as exact solution. Therefore, to simplify the calculation, we applied the assumption of the uniform flow field to the Ehara model.

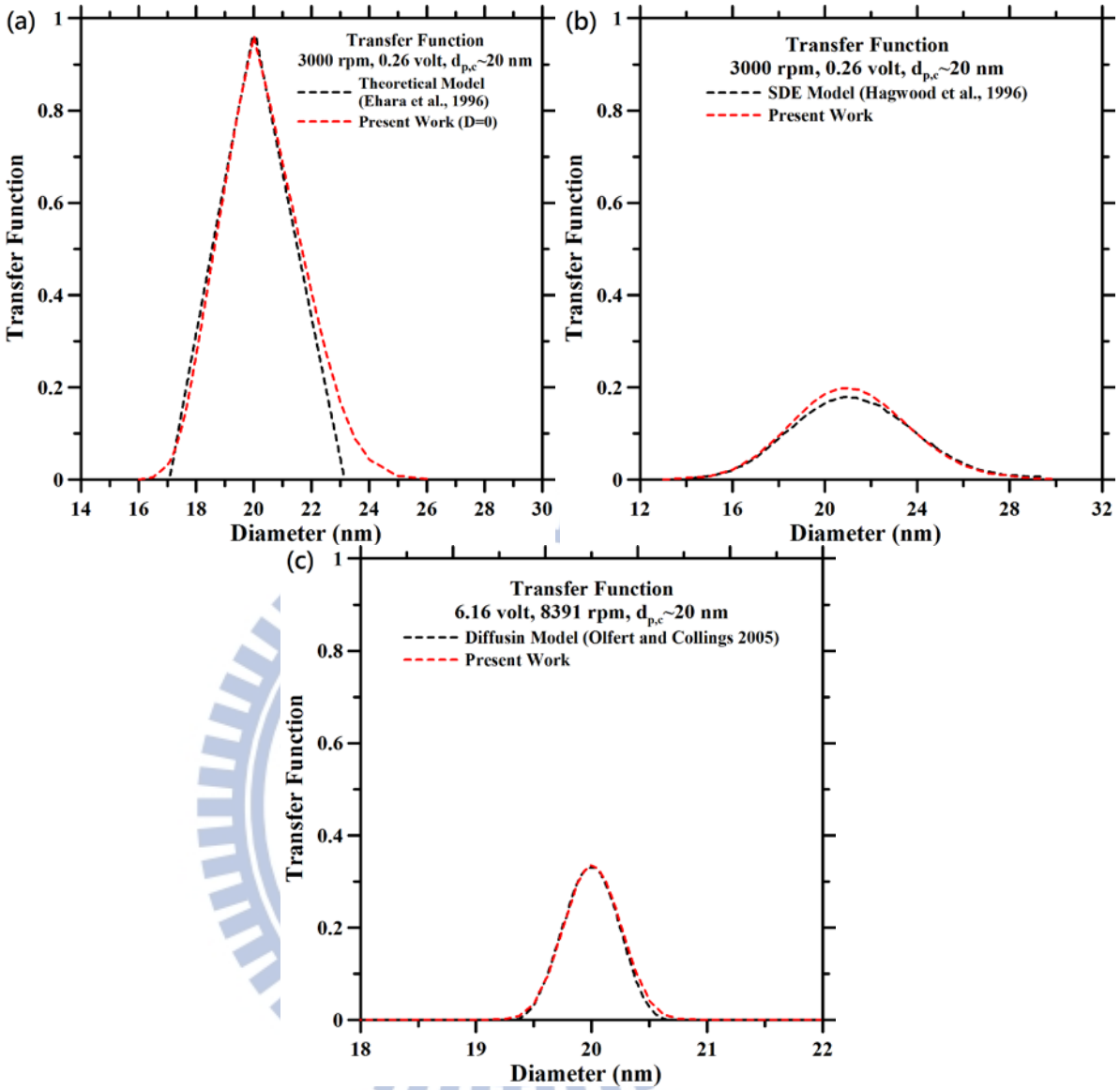

Fig. 8. The transfer function of comparing our model with (a) the theoretical model developed by Ehara et al., (1996), (b) the SDE model developed by Hagwood et al., (1995), (c) the diffusion model developed by Olfert and Collings (2005).

Fig. 8 shows the result of the comparisons. In Fig. 8(a), the dashed black line is obtained with our model, while the dashed red line is obtained with the theoretical model developed by Ehara et al., (1996). Since Ehara model neglected the Brownian motion, we zero the diffusivity of our model for making the comparison (D=0). The result showed good agreement between two models. In Fig. 8(b), the transfer function obtained with our model

(dashed red line) agrees very well with one simulated with the SDE model (dashed black line). The slight difference would be due to different principles or governing equations of the models. The SDE model is based on the escaped probability of particles whereas our model is based on the convection-diffusion equation. Fig. 8(c) shows the comparison of our model and the diffusion model developed by Olfert and Collings (2005). The transfer function simulated with our model is denoted as dashed red line, while the one simulated with the diffusion model is denoted as dashed black line.

In sum, the transfer functions simulated by our model agreed well with several models which were presented in previous studies. The good agreement is considered as the preliminary verification of the model. The verified model is considered as the representative of the previous models, whose calculation domain is the classifying region of the APM and the flow field is assumed parabolic.

3.3 Model with Extended Domain and Detailed Flow Profile

Although the model with classifying region domain and parabolic flow profile agrees very well with several previous studies, none of the previous models has agreed well with experimental data of nanoparticles even the model considered the diffusivity of particles. In other words, the model with classifying region and parabolic flow field cannot agree well with experimental data of nanoparicles as the troubles met in previous studies. We concluded that something might be wrong in the model. To improve the model, the model is advanced with two improvements. The first improvement is extending the calculation domain from the classifying region to all regions in the APM, and the second one is carefully considering the flow field in the APM.

The improvements are employed with two reasons. The first reason is that the calculation domain applied in previous models was the classifying region of the APM. However, particles classified by the APM pass through not only the classifying region but also

the inlet and outlet flow paths leading to the classifying region. Particles loss in these regions was ignored by previous studies due to the small calculation domain. The second reason is that rotation speed for nanoparticles is higher than that for submicron particles. The effects of the high rotation speed on the flow field would reduce the validity of the assumption of the parabolic flow field and lead the inaccuracy of the simulation. Hence, the more detailed consideration on the calculation domain and the flow field are applied to improve the model.

Calculation Domain

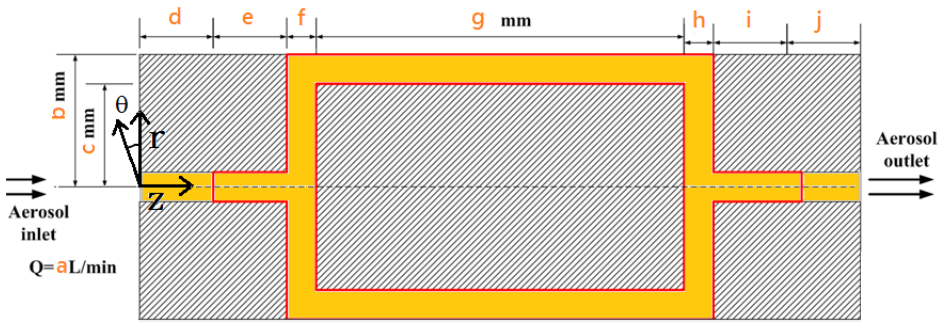

	3600	3601
a	1.0LPM	0.3LPM
b	52mm	25mm
c	50mm	24mm
d	63.5mm	64.5mm
e	114mm	73mm

	3600	3601
f	3.0mm	2.0 mm
g	250mm	100 mm
h	0.5mm	0.5 mm
i	255mm	88 mm
j	300mm	55.5 mm

3600 is original APM. 3601 is new one.

Fig. 9. The extended calculation domain (dark orange area) (Kanomax Inc.)

Fig. 9 shows the detailed geometry of the APMs. The dark orange area indicates the extended calculation domain. All regions where particles would pass through are considered in the model.

Flow Field

Instead of applying parabolic flow field for the velocity profile, the velocity profile in the calculation domain is calculated with the Navier-Stokes equations (Eq. (36)~(38)) and the continuity equation (Eq. (39)). We consider that the flow filed in the APM is steady. It is assumed that velocity would not change in the θ direction, which makes the 2-D consideration for the flow field available. Noted that u_θ, described by Eq. (40), appears in the Eq. (36). It reveals that the velocity in r direction (u_r) is affected by the rotation speed. S_u in the Eq. (38) is considered as the source term as described in Eq. (41). Since we consider the particles flow as the incompressible fluid, the continuity equation (Eq. (40)) is available to be applied to the flow field model.

$$\rho_{gas}\left(u_r\frac{\partial u_r}{\partial r}+u_z\frac{\partial u_r}{\partial z}\right)=-\frac{\partial P}{\partial r}+\mu_{gas}\left(\frac{\partial^2 u_r}{\partial r^2}+\frac{1}{r}\frac{\partial u_r}{\partial r}+\frac{\partial^2 u_r}{\partial z^2}\right)+\frac{\rho u_\theta^2}{r}-\frac{\mu u_r}{r^2} \tag{36}$$

$$\rho_{gas}\left(u_r\frac{\partial u_z}{\partial r}+u_z\frac{\partial u_z}{\partial z}\right)=-\frac{\partial P}{\partial z}+\mu_{gas}\left(\frac{\partial^2 u_z}{\partial r^2}+\frac{1}{r}\frac{\partial u_z}{\partial r}+\frac{\partial^2 u_z}{\partial z^2}\right) \tag{37}$$

$$\rho_{gas}\left(u_r\frac{\partial u_\theta}{\partial r}+u_z\frac{\partial u_\theta}{\partial z}\right)=-\frac{1}{r}\frac{\partial P}{\partial \theta}+\mu_{gas}\left(\frac{\partial^2 u_\theta}{\partial r^2}+\frac{1}{r}\frac{\partial u_\theta}{\partial r}+\frac{\partial^2 u_\theta}{\partial z^2}\right)+S_u \tag{38}$$

$$\frac{1}{r}\frac{\partial}{\partial r}\left(\rho_{gas} r u_r\right)+\frac{\partial}{\partial z}\left(\rho_{gas} u_z\right)=0 \tag{39}$$

$$u_\theta=\omega r \tag{40}$$

$$S_u=-\frac{\rho u_r u_\theta}{r}-\frac{\mu u_\theta}{r^2} \tag{41}$$

The equations are discretized by the finite volume method. The SIMPLER algorithm (Semi-Implicit Method for Pressure-linked Equation) (Patankar 1980) is used to solve the equations numerically (Lin et al., 2010). The numerical results of the flow field are applied to the advanced model for the calculation of the transfer function.

3.4 Simplified Model

Before applying model with detailed flow field to calculate the transfer function, the user has to spend lots of time on calculating the velocity profile of the field. Moreover, because the velocity profile is dependent on the rotation speed, flow rate and geometry of the APM, we have to calculate the velocity profile for each different operating condition. After that, we have to spend more time on calculating the transfer function. To simplifying the calculation process, the study develops the fitting model based on the numerical results to calculate transfer function in more efficient manner. Moreover, the study also applied numerical results to develop the modified Ehara model, which can calculate the transfer function as analytical solution. The two methods are described in following sections.

Fitting Model

The study builds up a fitting model, which is based on the numerical results simulated by the model with extended domain and detailed flow field. Gaussian distribution, as described in Eq. (42), is applied to fit the transfer function simulated by the developed numerical swirl model. Particle classified by the APM is considered to be spherical and singly charged, so the specific mass of particle can be easily converted to the diameter d_p.

$$d\Omega_{APM}(d_p, \omega_{\lambda c}, V) = \frac{X}{\sigma\sqrt{2\pi}} \exp\left(-\frac{(V-V_c)^2}{2\sigma^2}\right) dV \tag{42}$$

In Eq. (42), $\Omega_{APM}(d_p, \omega_{\lambda c}, V)$ is the transfer function of the particle, whose diameter is d_p, passing through the APM operated with rotation speed $\omega_{\lambda c}$ and voltage V. $\omega_{\lambda c}$ is the rotation speed determined based on the size of center particle ($d_{p,c}$) and the chosen λ_c (Eq. (4)), and V is the voltage applied to the APM. σ is the standard deviation of the voltage range that enable particle with diameter d_p to pass through the APM without being removed when

the rotation speed is fixed at $\omega_{\lambda c}$. The value of σ is obtained by trail and errors until the maximum difference between the fitted $\Omega_{APM}(d_p, \omega_{\lambda c}, V)$ and numerical $\Omega_{APM}(d_p, \omega_{\lambda c}, V)$ is minimized. Moreover, X is the correction factor, which not only normalizes the Gaussian distribution but also makes the maximum height of the Gaussian distribution equal to the maximum height of the numerical transfer function. V_c is the center voltage, derived from the rotation speed $\omega_{\lambda c}$ through equation. $\Omega_{APM}(d_{pc}, \omega_{\lambda c}, V_c)$ is the maximum transfer function when the APM is operated with $\omega_{\lambda c}$ and V_c. If the terms of σ and X are known, we can calculate the transfer function through Eq. (42) without additional numerical calculation.

Table 4 The results of fitting numerical transfer function with Gaussian distribution.

Gaussian Distribution Fits Numerical Models For APM-3600, 1 lpm, λ_c=0.22							
dp(nm)	**σ**	**V_c**	**Max abs. Error (in T.F.)**	**Sum of abs. Errors (in T.F.)**	**X**	**σ/V_c**	**V_c/σ**
20	0.399	2.10	0.032	0.290	0.284	0.190	5.263
30.6	0.800	4.79	0.026	0.150	0.989	0.167	5.988
51	2.150	12.70	0.050	0.525	3.407	0.169	5.907
100	6.690	43.24	0.027	0.270	12.694	0.155	6.463
208	20.840	143.63	0.026	0.170	42.029	0.145	6.892
479	63.330	454.17	0.026	0.320	130.071	0.139	7.171
791	115.910	832.75	0.028	0.380	239.431	0.139	7.184

In this section, the study chose the case of applying the APM-3600 to measure the mass distribution of particles with 0.22 of λ_c and 1 lpm of flow rate. Gaussian distribution is applied to fit seven different numerical transfer functions, which are simulated for particles with diameter 20 nm, 30.6 nm, 51 nm, 100 nm, 208 nm, 479 nm, 791 nm respectively. The

parameters, σ and X, is determined by trail and errors to minimize the maximum difference between the numerical transfer function and fitting Gaussian distribution. The obtained σ and X for each transfer function are listed in table 4. T.F. shown in table 4 is the abbreviation of the transfer function. The σ and X shown in table 4 are further fitted to predict the σ and X for size of particle which is not converted by the table. The fitting equation of σ and X are shown as below. The parameters, A,B,C,D,E, shown in Eq. (43)~(48) are listed in table 5 respectively. To remain the accuracy of the prediction, the digits of parameters after decimal point should not be rounded off.

Fitted σ:

For 208 nm > dp > 17 nm,

$$\sigma = A \times e^{(B \times d_p)} + C \times e^{(D \times d_p)} + E. \quad (43)$$

For 791 nm > d_p > 208 nm,

$$\sigma = A \times e^{(B \times d_p)} + C \times e^{(D \times d_p)} + E. \quad (44)$$

For d_p > 791 nm,

$$\sigma = 0.139 \times V_c. \quad (45)$$

Fitted X:

For 208 nm > dp > 17 nm,

$$X = A \times e^{(B \times d_p)} + C \times e^{(D \times d_p)} + E. \quad (46)$$

For 791 nm > d_p > 208 nm,

$$X = A \times e^{(B \times d_p)} + C \times e^{(D \times d_p)} + E. \quad (47)$$

For d_p > 840 nm

$$X = 239.431 + 0.3505126 \times (d_p - 791). \quad (48)$$

Table 5 The parameters of equations which are applied to fitted the obtained σ and X.

Fitted σ				Fitted X			
208 nm > d_p > 17 nm		791 nm > d_p > 208 nm		208 nm > d_p		840 nm > d_p > 208 nm	
A	17.9219737	A	83.6538647	A	77.0379673	A	-6.9615277
B	0.0039508	B	0.0017356	B	0.0024631	B	0.0037867
C	2.9876668	C	-11.6140818	C	10.0264075	C	169.7009613
D	-0.058499	D	0.0031225	D	-0.0259945	D	0.0014929
E	-19.9238423	E	-76.9483039	E	-86.6056268	E	-174.1644899

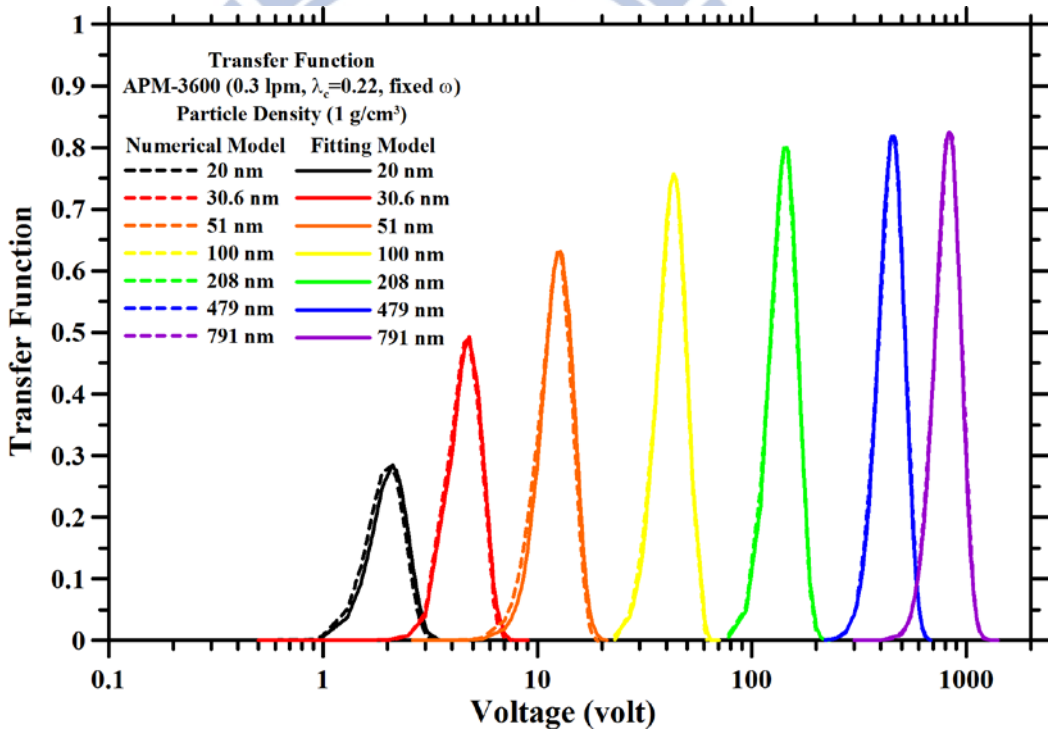

Fig. 10. Comparison between the numerical transfer function (solid lines) and the transfer function predicted by the fitting model (dashed lines)

To verify the fitting model, the transfer functions determined by the fitting model are compared with the fitted numerical transfer function. Fig. 10 shows the results of the

comparison. Good agreements are obtained and considered the verification of the fitting model. It should be keep in mind that because the fitted numerical transfer functions are simulated for the APM-3600 which is operated with 0.22 of the λ_c and 1lpm of the flow rate, the parameters shown in this section is only available for the APM-3600 operating with the same condition.

Modified Ehara Model

The study develops a modified Ehara model to calculate the transfer function as exact solution with considering the effects of Brownion motion. The model combines the model developed by Ehara et al., (1996) and the modified Gormley and Kennedy equation, which is modified based on our numerical results.

Ehara et al., (1996) developed a model (Ehara model) to calculate the transfer function of particles classified by the APM based. With the assumption of uniform flow field in the classifying region of the APM, Ehara model can calculate the transfer function as exact solution. Moreover, when the λ_c is sufficient low, the transfer function calculated with the uniform flow field can be very similar to the one calculated with the parabolic flow field, which is more close to the real flow field (Fig. 7). Hence, Ehara model was available to calculate the transfer function as exact solution without considerable error for the APM operated with low value of λ.

Fig. 11 is the typical transfer function calculated with the Ehara model with the uniform flow field. In Fig. 11, the shape of the transfer function can be determined by four special specific masses S_1^+, S_1^-, S_2^+, S_2^-. These specific masses can be calculated with Eq. (49) and (50) (Ehara et al., 1996). S_c is the specific mass of center particle (Eq. (51)), which achieves force balance of centrifugal force and electrostatic force at the center position ($r=r_c$) between the inner and the outer of the annular cylinders (classifying region).

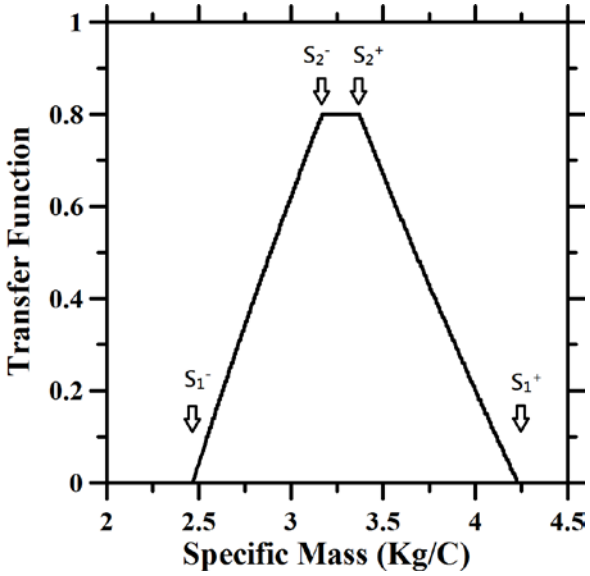

Fig. 11. Four particular specific masses

$$S_2^{\pm} \approx S_c\left(1 \pm 2\frac{\delta}{r_c}\right) \tag{49}$$

$$S_1^{\pm} \approx S_c\left[1 \pm 2\left(\frac{\delta}{r_c}\right)\coth\left(\frac{\lambda_c}{2}\right)\right] \tag{50}$$

$$S_c = \frac{V}{r_c^2\omega^2 \ln\left(\frac{r_2}{r_1}\right)} \tag{51}$$

Based on the specific mass S of particle, the transfer function $\Omega_{APM}(S)$ can be determined by three equations. If S ranges between S_1^- and S_2^-, Ω_{APM} (S) can be calculated with Eq. (52). Similarly, if S ranges between S_2^- and S_2^+, Ω_{APM} (S) can be determined by Eq. (53). If S ranges between $S_2^+ \le S \le S_1^+$, Ω_{APM} (S) can determined by Eq. (54). If S is out of these ranges, particle with such S will be completely removed by the APM.

For $S_1^- \le S \le S_2^-$ $(\rho_0^h = 1)$

$$\Omega_{APM}(S) = \frac{1}{2}\{[1-\rho(S)] + [1+\rho(S)]e^{-\lambda}\} \tag{52}$$

For $S_2^- \le S \le S_2^+$

$$\Omega_{APM}(S) = e^{-\lambda} \tag{53}$$

For $S_2^+ \le S \le S_1^+$ $(\rho_0^1 = -1)$

$$\Omega_{APM}(S) = \frac{1}{2}\{[1+\rho(S)] + [1-\rho(S)]e^{-\lambda}\} \quad (54)$$

$\rho(S)$ in Eq. (52)~(54) is the position of particles expressed in normalized coordinate as described by Eq. (55) and (56). r(S), derived from Eq. (1) is the position where centrifugal force and electrostatic force acting on particle of specific mass S are the same.

$$\rho(S) = \frac{[r(S)-r_c]}{\delta} \quad (55)$$

$$\zeta = \frac{z}{L} \quad (56)$$

$$r(S) = \sqrt{\frac{V}{S\omega^2 \ln\left(\frac{r_2}{r_1}\right)}} \quad (57)$$

To apply the Ehara model with considering the effects of Brownian motion, the study applied Gormley-Kennedy equation (Eq. (58)~(60)) to consider the effects of the Brownian motion of particles on the transfer function. It is assumed that the diffusion loss of particles is independent to the classification of the APM. In other words, the study applies the product of Ω_{APM} (S) and $P_{G\&K}$ to calculate the transfer function of nanoparticles. In the study, Ehara model modified by the diffusion loss equation is denoted as the Modified Ehara model, and the transfer function calculated with the modified Ehara model is denoted as $\Omega'_{APM}(S)$.

$$\mu = \frac{\pi DL(r_2+r_1)}{Q((r_2-r_1))} \quad (58)$$

$$P_{G\&K} = 1 - 2.96\mu^{\frac{2}{3}} + 0.4\mu \quad \text{for } \mu<0.005 \quad (59)$$

$$P_{G\&K} = 0.910\exp(-7.54\mu) + 0.0531\exp(-85.7\mu) \quad \text{for } \mu \geqq 0.005 \quad (60)$$

D: The diffusivity or diffusion coefficient (m^2/s)

Q: The flow rate of the flow entering the APM (m^3/s)

$P_{G\&K}$: The penetration of particles passing through the APM

To verify Gormley and Kennedy equation, we applied the equation to predict the penetration of nanoparticles passing through the classifying region of the still APM (0 rpm, 0 volt). Then, the penetrations predicted are compared to the numerical ones simulated with our numerical model with extended domain and detailed flow field as reference. Because neither centrifugal force nor electrostatic force occurs in the still APM, it is considered that the penetration of nanoparticles is mainly due to the diffusion loss. The validity of the numerical penetrations has been checked with experimental data presented in Tajima et al., (2011), which will be mentioned in next chapter "4.1 Diffusion Loss Prediction".

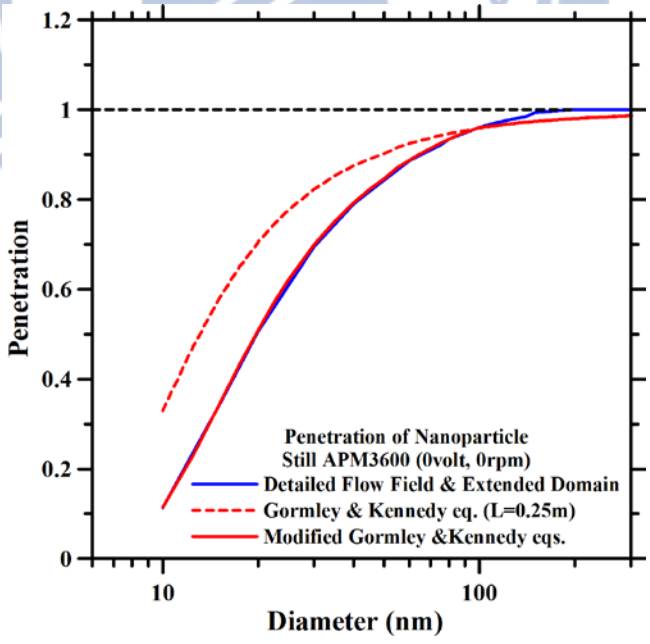

Fig. 12. The calculated penetration of particles passing through the still APM.

Fig. 12 shows the results of the simulation. The dashed red line is the penetration

calculated with Gromley and Kennedy equation (L=0.25 m) and the solid blue line is the numerical penetration simulated with our numerical model. It is found that Gormley and Kennedy equation significantly overestimate the penetration of nanoparticles. The degree of the overestimation increases for smaller nanoparticles (increases from 0% to 20% or more on penetration). We conclude that the overestimation is due to Gormley and Kennedy equation consider the classifying region of the APM only, while the numerical model considers whole the region of the APM. More discussions are in chapter "4.1 Diffusion Loss Prediction".

Instead of extending the calculation domain of Gormley and Kennedy equation (still not be accurate after the try), we apply another correction factor K to modify the $P_{G\&K}$ directly as described in Eq. (61). The correction factor K is a function of particle size, which is described in Eq. (62) and (63). The function is obtained by fitting the difference between the $P_{G\&K}$ and the numerical penetration for several sizes of nanoparticle. The penetrations calculated with the modified Gormley and Kennedy equation (solid red lines) agree very well with numerical penetration (Fig. 12). Hence, the modified Gromley and Kennedy equation is applied to modified Ehara model as described in Eq. (64).

$$P'_{G\&K} = K \times P_{G\&K} \tag{61}$$

For d_p smaller than 100 nm or equal to 100 nm

$$K = -1.64 \times \exp(-0.14 \times d_p) - 0.36 \times \exp(-0.03 \times d_p) + 1.02 \tag{62}$$

For d_p larger than 100 nm

$$K = 1 \tag{63}$$

$$\Omega'_{APM}(S) = \Omega_{APM}(S) \times P'_{G\&K} \tag{64}$$

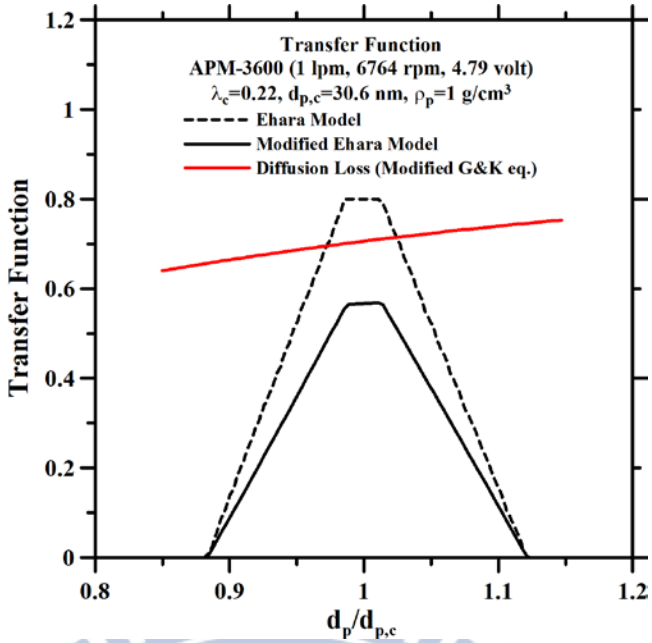

Fig. 13. The transfer functions are calculated with Ehara model (dashed black line) and modified Ehara model (solid black line). The modified Gormley and Kennedy equation applied in modified Ehara model is dented as solid red line.

After modifying Gormley and Kennedy equation, The transfer function calculated with the modified Ehara model is compared with the one calculated with the Ehara model. Fig. 13 shows the result of the comparison. The dashed black line is the transfer function calculated with the Ehara model, and the solid black line is the transfer function calculated with the modified Ehara model. The height difference of the transfer functions is due to the modified Gormley and Kennedy equation (solid red line), which represents the diffusion loss of particles in the APM.

4 Results

After building up the models (the model with classifying region domain parabolic flow profile and the model with whole region domain and detailed flow profile), the models are compared to study the accuracy of the prediction. The effects of the extended calculation

domain and the detailed flow field are considered by comparing the models with the experimental data.

4.1 Diffusion Loss Prediction

The model with extended domain and detailed flow field is applied to predict the penetration of nanoparticles passing through the still APM (0 volt, 0 rpm). Because there is no centrifugal force and electrostatic force in the still APM, particles lost in the APM are expected to be due to the diffusion loss. The predicted penetrations are also compared with the ones predicted by the model with classifying region domain and parabolic flow field. Moreover, these theoretical results are compared with the experimental penetration presented in Tajima et al., (2011), who measured the penetration of monodisperse particles passing through the still APM (Model-3600, Kanomax Inc.).

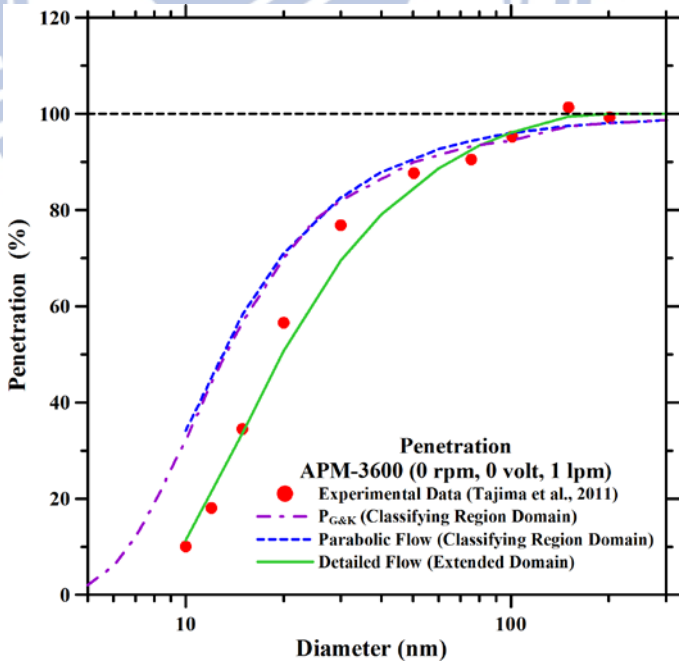

Fig. 14. The penetration of particles passing through the still APM-3600

Fig. 14 shows the result of comparison. Points in the Fig. 14 are the experimental data

presented in Tajima et al., (2011). The dashed blue line is the results simulated with the model with classifying region domain and parabolic flow field, while the solid green line is the results simulated with the model with whole domain and detailed velocity profile. The latter model accurately predicts the penetration of nanoparticles; in contrast, the former model overestimates the experimental data significantly. The overestimation is due to the insufficient calculation domain (classifying region) which cannot describe the diffusion loss of particles in the APM completely.

Gormley and Kennedy equation (Hinds 1999) is a well known equation that can predict the penetration of particles passing through the tube, tunnel or annular cylinder. We applied the Gormley and Kennedy equation, as mentioned in chapter 3.4 (Eq. (58)~(60)), to calculate the penetration of particles passing through the still APM-3600. L is considered the length of the classifying region of the APM (0.25 m). In Fig. 14, the penetration predicted with the Gormley and Kennedy equation is denoted as dashed dotted purple line. It should be noted that the results simulated by the Gormley and Kennedy equation are almost same as ones simulated by the model with classifying region and parabolic flow profile. It is the evidence showing particles loss in the classifying region of the still APM is mainly due to the diffusion loss. Hence, insufficient calculation domain would answer the question that why previous studies (Olfert et al., 2006, Lall et al., 2009) significantly overestimated the experimental data of nanoparticles even though their model had considered the diffusivity of particles.

Comparing to the model with classifying region domain and parabolic flow profile, the model with extended domain and detailed flow field consideration has better accuracy on prediction the penetration of particles passing through the still APM. The maximum inaccuracy of prediction is reduced from about 20% to 10% in penetration. In sum, the extended calculation domain significantly improves the accuracy of the model.

4.2 Recirculation Flow

The section studies the effects of the parabolic flow field and detailed flow field on the transfer functions of nanoparticles and submicron particles. The calculation domain applied to the model is the classifying region of the APM-3601. The parabolic flow field and the detailed flow field determined by the Navier-Stoke equations (as described in Eq. (36)~(41)) are applied to the model to calculate the transfer function respectively.

Fig. 15 shows the transfer functions of nanoparticles. The dashed lines are the transfer functions simulated with the parabolic flow field, while the solid lines are the transfer functions simulated with the detailed flow field. All the solid lines are lower than the dashed lines, which show the enhanced loss due to different types of flow field. The enhanced loss for each rotation speed is 3% (11227 rpm, 40 nm), 5% (13143 rpm, 30 nm) in transfer function respectively. Fig. 16 is the transfer functions of submicron particles (200 nm). The dashed and solid lines are the transfer functions calculated with parabolic flow field and detailed flow field respectively. They are almost same, which are not affected by the different flow field.

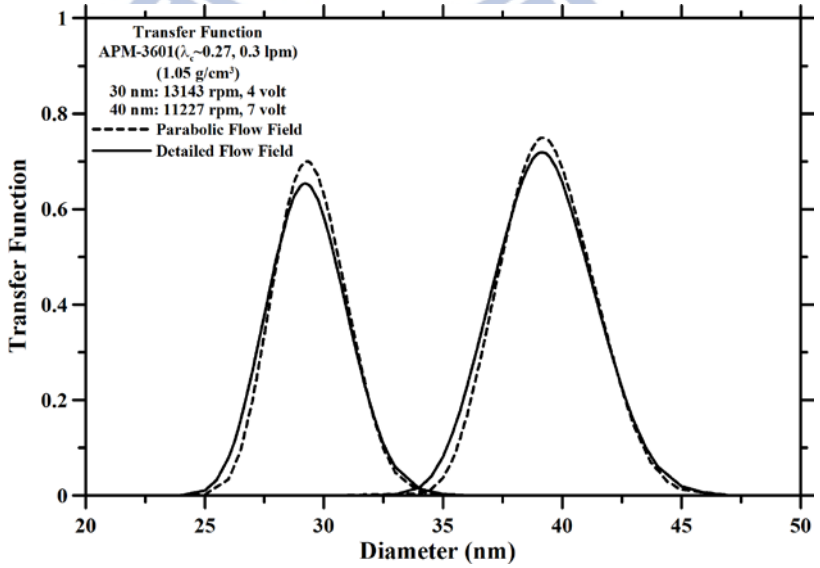

Fig. 15. The transfer functions of nanoparticles are simulated with parabolic flow field (dashed lines) and detailed flow filed (solid lines) respectively.

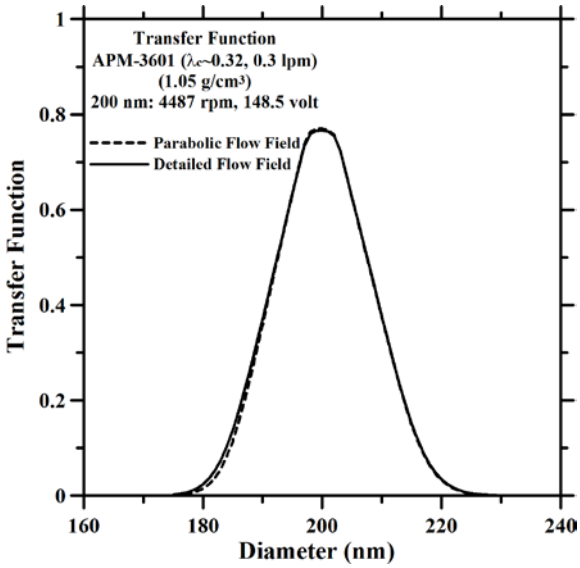

Fig. 16. The transfer functions of submicron particles are simulated with parabolic flow field (dashed lines) and detailed flow filed (solid lines) respectively.

The effects of the different flow fields on the transfer functions are summarized in table 6. $\Omega_{para.max}$ and $\Omega_{detail.max}$ denote the maximum height of the transfer functions calculated with parabolic and detailed flow field respectively. It is found that the enhanced loss of the transfer functions is increased with higher rotation speed.

Table 6 The heights of the transfer functions calculated with different flow field.

λ_c	rpm	dp (nm)	$\Omega_{para,\ max}$	$\Omega_{detail,\ max}$	Enhanced Loss
0.32	4487	200nm	0.77	0.77	0.00
0.27	11227	40nm	0.75	0.72	0.03
0.27	13143	30nm	0.70	0.65	0.05
Calculation Domain: Classifying region					

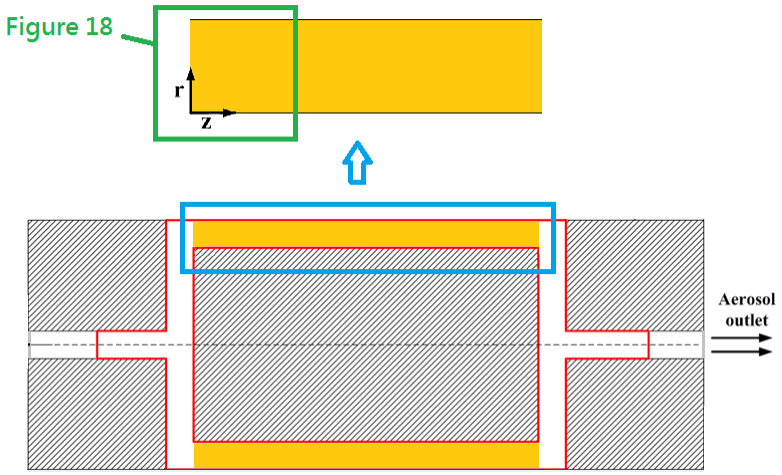

Fig. 17. The front region of the classifying region (Marked by green rectangular)

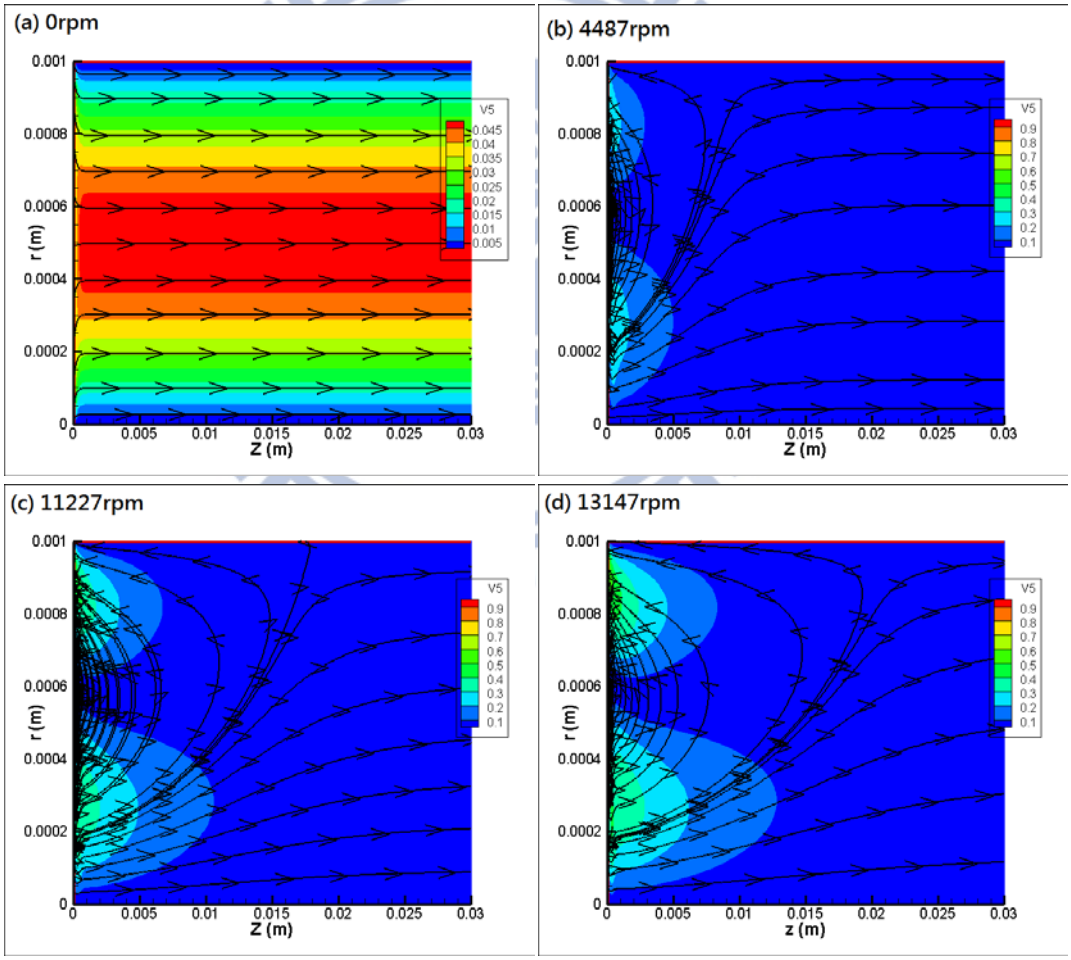

Fig. 18. The flow filed at the front region of the classifying region of the APM-3601 rotating with (a) 0 rpm, (b) 4487 rpm, (c) 11227 rpm, and (d) 13147 rpm. V5 denotes velocity (m/s).

In addition, according to the velocity profile of the detailed flow filed, we find that recirculation flow occurs in the classifying region (the region marked by green rectangular Fig. 17). Fig. 18 shows detailed velocity profile and the streamlines of the region. For the still APM (0 rpm), the flow filed of the region is very similar to the parabolic flow field. In contrast, for the rotating APM, the counterclockwise recirculation flow appears in the region. The scale of the recirculation flow increases with greater rotation speed due to the stronger forced vortex. On the other hand, there is no recirculation flow in parabolic flow field because the flow in the region has no velocity in r direction. Hence, we conclude that the enhanced losses of transfer functions as shown in Fig. 15 are due to the enhanced convection-diffusion deposition caused by the recirculation flow, which cannot be considered with the parabolic flow filed.

4.3 APM Response Spectra

The APM response spectra or normalized particle concentration are the ratios of particle concentration at the APM outlet to particle concentration at the APM inlet. The section applies the transfer functions calculated with our fitting model and modified Ehara model to calculate the APM response spectra respectively. Furthermore, the response spectra are compared to the experimental ones presented in Tajima et al., (2011) as verification.

Response Spectra

Fig. 19 shows the scheme of DMA-APM measurement system to which Tajima et al., (2011) used measure the experimental response spectra. Size standard particles (Duke Inc.) are neutralized before enter DMA. Then, the particles are monodispersed by the DMA and classified by the APM. The experimental response spectra are calculated based on the particle concentration measured by the Condensed Particle Counter (CPC). The system can

be expressed mathematically as described in previous studies (Ehara et al., 1996, Lall et al., 2009, Tajima et al., 2011). The neutralizer is not included in the calculation because it is assumed that size distribution of the size standard particles is so narrow (Duke Inc.) that it is not affected by the neutralization. Eq. (65) and (66) describe the particles classified by the DMA-APM system in the specific mass form and particle size form respectively.

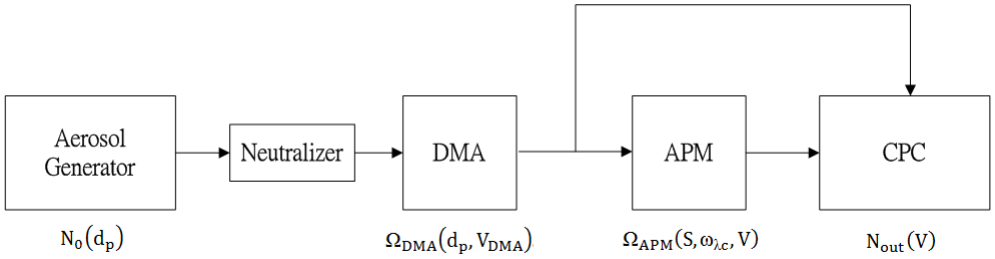

Fig. 19. The scheme of DMA-APM measurement system

$$N_{out}(V) = \int N_0(d_p)\Omega_{DMA}(d_p, V_{DMA})\Omega_{APM}(S, \omega_{\lambda c}, V)\, dS \quad (65)$$

$$N_{out}(V) = \int N_0(d_p)\Omega_{DMA}(d_p, V_{DMA})\Omega_{APM}(d_p, \omega_{\lambda c}, V)\, dd_p \quad (66)$$

In Eq. (65) or Eq. (66), $N_0(d_p)$ is the size standard particle (PSL), which is considered Gaussian distribution with standard deviation and mean diameter provided by the manufacturer of the PSL (JSR Corp.). Before entering the APM, particles are classified by the DMA so the size distribution becomes sharper (monodisperse). We applied the theoretical transfer function of the DMA (Stolzenburg and McMurry 2008), denoted as $\Omega_{DMA}(d_p, V_{DMA})$, to describe the classification of the DMA. V_{DMA} is the voltage applied to the DMA, and the d_p is the chosen size of the monodisperse particles. Then, monodisperse particles are classified by the APM. Similarly, we describe the classification of the APM with the transfer function $\Omega_{APM}(d_p, \omega_{\lambda c}, V)$, which are calculated with our fitting model and modified Ehara model respectively. For example, if we are going to measure the mass distribution of 30.6nm monodisperse particles with 0.22 of λ_c, the $\omega_{\lambda c}$ can be calculated based

on the chosen λ_c (described by Eq. (4)) and the relaxation time of the 30.6 nm particle. Then, the rotation speed is fixed at $\omega_{\lambda c}$, while the voltage V is shifted to scan or measure the specific mass distribution (or mass distribution) of the particles. Then, particles passing through the DMA-APM measuring system is described by $N_{out}(V)$, which is the number concentration of particles at the outlet of the APM. Finally, the response spectra, which are the function of V, can be calculated with Eq. (67). The calculated response spectra are compared to experimental one presented in Tajima et al., (2011).

$$\text{Response Spectra}(V) = \frac{N_{out}(V)}{\int N_0(d_p)\Omega_{DMA}(d_p,V_{DMA})dd_p} = \frac{N_{out}(V)}{\int N_{in}(d_p)dd_p} \quad (67)$$

It should noted that the calculation presented in the section is only available for spherical particles because their specific mass S and diameter d_p can be converted to each other easily. If particles are non-spherical (ex: carbon nanotube), the calculation presented in the study would be inadequate, which is not discussed in the thesis. The thesis prefers the size of the particles (Eq. 66) because it is more intuitive to describe a small particle with its size. The calculated response spectra are shown in Fig. 20 ~ 22, and each set of points in the figures are the experimental response spectra presented in Tajima et al., (2011).

In Fig. 20, the response spectra are calculated with the transfer function done with our fitting model. The calculated response spectra agree very well with the experimental ones. The height difference between the calculated transfer function and experimental transfer functions are less than 6% in normalized particle concentration (response spectra). The results show the validity of the fitting model.

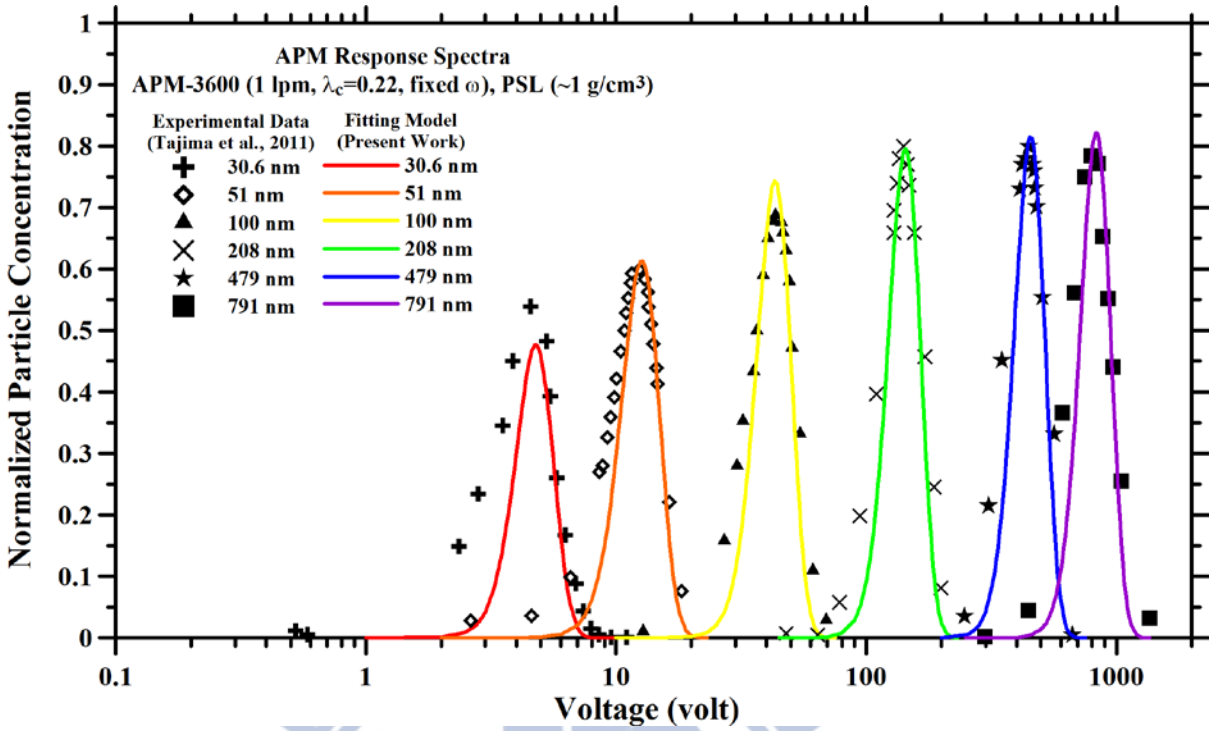

Fig. 20. The APM response spectra calculated with fitting model. (λ_C=0.22)

In Fig. 21 and 22, the response spectra are calculated with both modified Ehara model and Ehara model for λ_c=0.2 and λ_c=0.49 respectively. For the modified Ehara model, the calculated response spectra of both nanoparticles and submicron particles are very close to the experimental ones. For the case of λ_c=0.22 and λ_c=0.49, the maximum height difference between the calculated and experimental response spectra is less than 5% and 10% in response spectra respectively. For Ehara model, the calculated response spectra of submicron particles agree well with experimental ones, whereas the response spectra of nanoparticles overestimate the experimental ones significantly. For the case of λ_c=0.22 and λ_c=0.49, the maximum difference between the calculated and experimental response spectra is about 20% and 17% in response spectra respectively. The significant overestimations is due to Brownian motion of particle is neglected by Ehara model. After the Ehara model is modified by the modified Gromley and Kennedy equation, the overestimation of response spectra of nanoparticles is improved significantly.

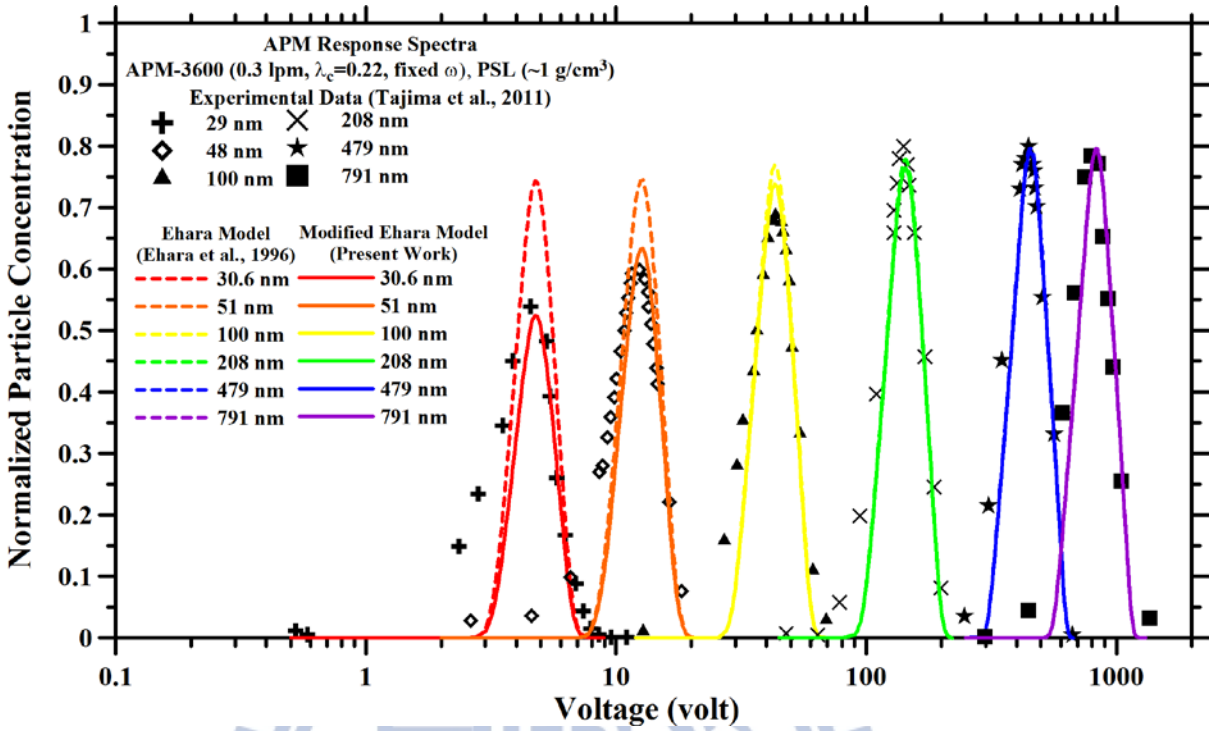

Fig. 21. The response spectra calculated with the modified Ehara model. (λ_C=0.22)

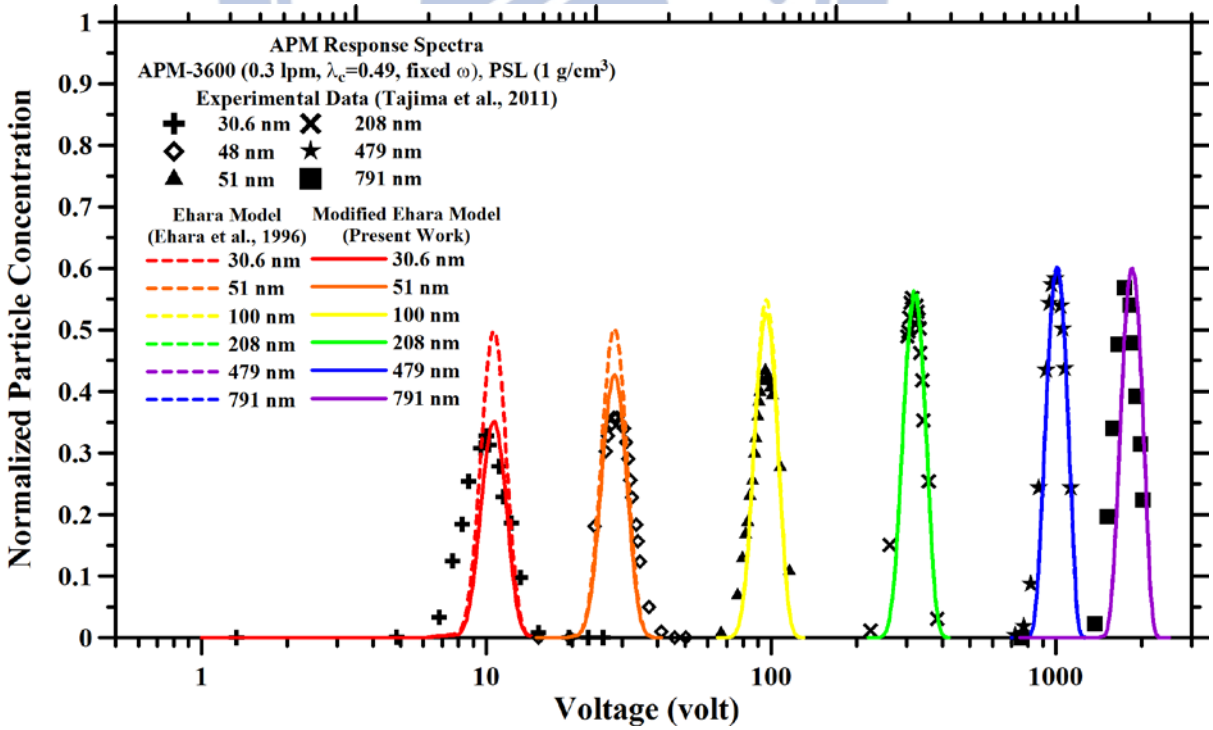

Fig. 22. The response spectra calculated with the modified Ehara model. (λ_C=0.49)

Table 7 and table 8 summarize the accuracy of the tested models. For submicron particles, all the calculated response spectra agree well with the experimental ones for both operating conditions (λ_c=0.22 and λ_c=0.49). In contrast, for nanoparticles, the response spectra calculated with Ehara model overestimate the experimental ones, while both the fitting model and the modified Ehara model still agree very well with the experimental data of both nanoparticles and submicron particles. The differences the height of the response spectra between the calculated results and the experimental data are less than about 10%, which shows the validity of the fitting model and the modified Ehara model.

Table 7 The difference between the heights of the calculated response spectra and experimental response spectra (λ_c=0.22).

λ_c=0.22				
PSL	**APM-3600**	**Difference in Height of the Reponse Spectra**		
d_p (nm)	**rpm**	**Ehara Model**	**Fitting Model**	**Modified Ehara Model**
30.6	6764	0.20	-0.06	-0.02
51	5117	0.14	0.02	0.03
100	3439	0.08	0.07	0.05
208	2089	-0.02	-0.01	-0.04
479	1063	0.00	0.01	-0.01
791	678	0.02	0.05	0.01

Table 8 The difference between the heights of the calculated response spectra and experimental response spectra (λ_c=0.49).

λ_c=0.49			
PSL	**APM-3600**	**Difference in Height of the Reponse Spectra**	
d_p (nm)	**rpm**	**Ehara Model**	**Modified Ehara Model**
30.6	10095	0.17	0.02
51	7636	0.14	0.07
100	5132	0.12	0.10
208	3118	0.02	0.01
479	1587	0.02	0.02
791	1012	0.03	0.03

Notice and Restrictions of the Models

This paragraph describes the notice to ensure the validity of the simplified models as well as the restriction of the models. As mentioned in chapter 3.4, the parameters applied to the fitting model are dependent on the model of the APM applied in the experiment, the value of λ_c, and the flow rate in the APM. The parameters of the fitting model presented in the thesis are only available to the APM-3600 which is operated with 0.22 of λ_c and 1lpm of flow rate in the APM. If λ_c or the flow rate is changed, user has to produce another set of numerical transfer functions based on the whole domain of the APM and detailed flow field to update the parameters of the fitting model. Fortunately, the flow rate of the APM-3600 and APM-3601 are usually set at 1 lpm and 0.3 lpm respectively, so the parameters would be mainly based on the value of λ_c. When applying the modified Ehara model, the calibrating factor K presented in the thesis, which depends on the geometry of the APM, is only available for the APM-3600 operated with 1 lpm of flow rate. If one applied different model of the APM or different flow rate, the factor K should be newly modified with corresponding numerical results which are calculated by our detailed numerical model, as we did in Fig. 12. Compared to the fitting model, we don't have to change K factor of the modified Ehara model when we operate the APM with various λ_c. The response spectra presented in the thesis is calculated with ideal size distribution of monodisperse particles. The ideal assumption may lead the discrepancy between the calculated results and experimental ones. For example, it is found that the calculated response spectra are narrower than the experimental one, which is probability due to the size distributions of particles applied in the calculation (ideal sharp distribution) are different to the ones actually presented in the experiments (actual distribution). Another example is that the calculation is based on the assumption that all the particles passing through the APM are singly charged. In experiments, some of particles would be multiply charged, which will lead more particles loss in the APM and results in the

lower experimental response spectra compared to the experimental ones. Despite of the fact that the calculated response spectra may be different to the experimental one, some of the problem could be solved or eased with more detailed consideration (ex: applied experimental size distribution of particles for response spectra), the calculated response spectra still can be the references for the researchers.

5 Conclusion

A 2-D numerical APM transfer function model is successfully constructed based on the governing equation of convection-diffusion equations and continuity equation. Three dimensionless numbers, which can cover ones presented in previous studies, are obtained from the governing equation of the model. These dimensionless numbers could be applied to characterize the performance of the APM.

Different calculation domains and flow fields applied to the model are discussed in the thesis. When the transfer function model is coupled with extended calculation domain (whole region in the APM) and detailed flow field, the accuracy of predicting the penetration of nanoparticles passing through the still APM is significantly increased compared to that coupled with classifying region and parabolic flow field. The maximum overestimations of the predictions are significantly reduced from 20% to 10%. The significant improvement shows that diffusion loss of particles occurs not only in the classifying region but also in the inlet and outlet paths leading to the classifying region. We concluded that the calculation domain of the transfer function model should be extended from classifying region to the whole region of the APM.

In addition, enhanced loss of particles is found when applying detailed flow field to the transfer function model. Under the similar λ_c, smaller nanoparticles have greater enhanced loss, while submicron particles have no enhanced loss. The study concludes that the

enhanced is due to the recirculation flow found in the velocity profile of the detailed flow field, and the scale of recirculation flow is increased with higher rotation speed.

Two transfer function models, the fitting model and the modified Ehara model, are developed to calculate the transfer function in a more convient manner compared to the numerical model. The former is developed by fitting the numerical results of transfer functions considering the whole calculation domain and detailed flow field, while the latter is developed by modifying Ehara model using the modified Gormley and Kennedy equation which is based on numerical convection-diffusion particle loss. These models are applied to calculate the APM response spectra of the DMA-APM mass measurement system. Compared to the experimental response spectra, the maximum inaccuracies of calculated response spectra are less than 10% in normalized particle concentration. The results show the validity of the transfer function models.

According to the results of the thesis, we expect that accurate real time mass distribution measurement of both nanoparticles and submicron particles can be realized in the future.

Reference

Aerosol Instrument Manager® Software for Scanning Mobility Particle Sizer™ (SMPS™) Spectrometer (2010). TSI.

Aerosol Particle Mass Analyzer, Model 3601 APM-II, Kanomax USA Inc.

Lall, A.A., Ma, X., Guha, S., Mulholland, G.W., and Zachariah, R.M. (2009). Online Nanoparticle Mass Measurement by Combined Aerosol Particle Mass Analyzer and Differential Mobility Analyzer: Comparison of Theory and Measurements, *Aesosol. Sci. Technol.* 43:1075-1083.

Hagwood, C., Coakley, K.J., Negiz, A., and Ehara, K. (1995). Stochastic Modeling of a New Spectrometer, *Aesosol. Sci. Technol.* 23:611-627.

Lin, G.Y. and Tsai, C.J. (2010). Numerical Modeling of Nanoparticle Collection Efficiency of Single-Stage Wire-in-Plate Electrostatic Precipitators. *Aesosol. Sci. Technol.* 44:1122-1130.

Hinds,W. C.. Aerosol Technology (JohnWiley & Sons, New York, 1999). Second edition. 166.

Ehara, K., Hagwood, C. and Coakley, K.J. (1995). Motion of Charged Aerosol Particles Under Coexistence of Electrostatic and Centrifugal Forces. *Japan Association of Aerosol Sci. Technol*. 10:51-53.

Ehara, K., Hagwood, C. and Coakley, K.J. (1996). Novel Method To Classify Aerosol Particles According to Their Mass-To-Charge Ratio-Aerosol Particle Mass Analyzer. *J. Aerosol Sci.* 27:217-234.

Olfert, J.S., Collings, N., (2005). New method for particle mass classification-the Couette centrifugal particle mass analyzer. *J. Aerosol Sci.* 36:1338-1352.

Olfert, J.S., Reavell, K.StJ., Rushton, M.G. and Collings, N. (2006). The experimental transfer function of the Couette centrifugal particle mass analyzer. *J. Aerosol Sci.* 37:1840-1852.

Patankar, S. V. (1980). *Numerical Heat Transfer and Fluid Flow*. Hemisphere, New York.

Product Information- Model 3080-Series Electrostatic Classifiers. TSI.

Series 3080 Electrostatic Classifiers-Operation and Service Manual. TSI.

Stolzenburg, M. R. (1988). An Ultrafine Aerosol Size Distribution Measuring System. *Department of Mechanical Engineering, University of Minnesota*, Minneapolis, MN.

Tajima N., Fukushima N., Ehara K., and Sakurai H. (2011). Mass Range and Optimized Operation of the Aerosol Particle Mass Analyzer. *Aesosol. Sci. Technol.* 45:196–214.

Tajima N., Ehara K., Sakurai H., Fukushima N. Miniaturization of the Aerosol Particle Mass Analyzer (APM). Kanomax corp. and AIST (National Institute of Advanced Induxtrial Science and Technology).

Appendix A Some Properties of Previous Models

Transfer Function Model (Ehara et al., 1996)

Based on 5 assumptions

a) The particles introduced in the classifying region of the APM rotated at the same angular velocity as the classifying region (annular cylinders).

b) The particle inertia, Brownian motion, the interaction between aerosol particles, and the image potential were neglected. The drag force is balanced by the electrostatic and centrifugal force

c) It is assumed that there was no flow in r and θ direction. The flow is in z direction only. Flow field in the classifying region was steady.

d) The Coriolis force was neglected due to the primary motion of the particles was parallel to the axis of rotation.

e) The distance between the inner and outer electrodes was assumed to be much smaller than their radii. (r_2, $r_1 >> r_2 - r_1$)

Transfer Function Model (Hagwood et al. 1995)

Laminar flow, spherical particles, uniform density

a) Stochastic Differential Equations(SDE)

- Deriving PDE from the concept of escape probability of particle.
- The Brownian motion in z direction was neglected (along the flow direction).
- Solving PDE with a finite difference discretization along the r direction. (The complete discussions can be refer to Kahaner et al. (1989), solved by FORTRAN)

b) Monte Carlo Approach (MC)

- The SDE which govern the aerosol trajectory was a Langevin equation. A Monte Carlo method like that described in Risken (1984) was applied to solve the

Langevin equation.

- Considering the Brownian motion both in z and r direction; hence, it can consider the diffusion broadening effect and diffusion loss simultaneously.
- MC Model needs more computation time compared to SDE Model.

Appendix B The Geometry of Classifying Region of the APM Applied in Previous Studies

The geometry of classifying region of the APM applied in previous studies.

Geometry of Classifying Region of the APM Applied in Previous Studies													
	Geometry of APM			Operating Condition					DMA			Aerosol	
APM Model	**r_{inner} (m)**	**r_{outer} (m)**	**Length of APM (m)**	**Air Flow Rate (lpm)**	**Retention Time (s)**	**Rotation (rpm)**	**Pressure (atm)**	**Temp. (˚C)**	**DMA Model**	**Q_{sheath} (LPM)**	**$Q_{aerosol}$ (LPM)**	**Material**	**$\rho_{aerosol}$ (Kg/m^3)**
Ehara et al., (1996) Prototype APM	0.1	0.103	0.2	0.5	45.918		atmospheric. (assumed 1)	room (assumed 25)				PSL	1000
Hagwood et al., (1995) Virtual APM	0.1	0.101	0.2	0.5	15.155	3000	atmospheric. (assumed 1)	room (assumed 25)					1000
Olfert and Collings (2005) Virtual APM	0.1	0.103	0.2	0.5	45.918		atmospheric. (assumed 1)	22					1000
Lall et al., (2009) APM-10 Kanomax	0.05	0.052	0.25	0.3 (N_2)	32.044		atmospheric. (assumed 1)	room (assumed 25)	TSI Model 3081 (Long)	3~5	0.3	PSL	1050
Tajima et al., (2011) APM-3600 Kanomax	0.05	0.052	0.25	1	9.613		atmospheric. (assumed 1)	room (assumed 25)	TSI Model 3071 or 3081 (Long)	10	1	PSL, NaCl	1000
NCTU, Nanoparticle and Air Quality Laboratory, 2012~ APM-3601 Kanomax	0.024	0.025	0.1	0.3	3.079		1	25	TSI Model 3081 (Long)	9	1.1	PSL, Silver	1050